Caspar determines primordial germ cell identity in *Drosophila melanogaster*

Subhradip Das[1,#], Sushmitha Hegde[1,#], Neel Wagh[1], Jyothish Sudhakaran[1], Adheena Elsa Roy[1], Girish Deshpande[1,2,*] & Girish S Ratnaparkhi[1,*]

[#]Equal Contribution

[1]Department of Biology, Indian Institute of Science Education & Research, Pune, INDIA

[2] Department of Molecular Biology, Princeton University, Princeton, NJ 08544, USA Princeton University,

[*]Author(s) for Correspondence: girish@iiserpune.ac.in (GR), gdeshpande@princeton.edu (GD)

ORCID IDs: SH (0000-0003-0777-962X); SD (0009-0002-4553-966X); AR (0009-0008-6000-9572); NW (0009-0006-0639-6116), JS (0000-0001-5828-5182); GR (0000-0001-7615-3140), GD (0000-0002-5200-7090)

Running Title. Caspar: A Novel Germ Cell Determinant.

Figures: 10

Suppl. Material: 4

Abstract

Repurposing of pleiotropic factors during execution of diverse cellular processes has emerged as a regulatory paradigm. Embryonic development in metazoans is controlled by maternal factors deposited in the egg during oogenesis. Here, we explore maternal role(s) of Caspar (Casp), the *Drosophila* orthologue of human Fas-associated factor-1 (FAF1) originally implicated in host-defense as a negative regulator of NF-κB signaling. Maternal loss of either Casp or it's protein partner, Transitional endoplasmic reticulum 94 (TER94) leads to partial embryonic lethality correlated with aberrant centrosome behavior, cytoskeletal abnormalities, and defective gastrulation. Although ubiquitously distributed, both proteins are enriched in the primordial germ cells (PGCs), and in keeping with the centrosome problems, mutant embryos display a significant reduction in the PGC count. Moreover, the total number of pole buds is directly proportional to the level of Casp. Consistently, it's 'loss' and 'gain' results in respective reduction and increase in the Oskar protein levels, the master determinant of PGC fate. To elucidate this regulatory loop, we analyzed several known components of mid-blastula transition and identify the translational repressor Smaug, a zygotic regulator of germ cell specification, as a potential critical target. We present a detailed structure-function analysis of Casp aimed at understanding its novel involvement during PGC development.

Keywords: Fas-associated factor 1, Germ plasm, Valosin Containing Protein, Maternal, Pole cell, Vasa, P97, MZT, ZGA.

Introduction

As a model organism, *Drosophila melanogaster*, has been instrumental in establishing and advancing several developmental paradigms underlying embryonic development. In recent years, it has also emerged as a relatively simple yet tremendously useful model, to analyze the underpinnings of the immune response (MEDZHITOV 2001; LEMAITRE AND HOFFMANN 2007). Critically, despite the small size and modest cellular complexity, the insect immune system shares many fundamental traits with the higher vertebrates, including the humoral and innate arms and the dialogue between the two (HULTMARK 1993; ADAMS *et al.* 2000). Furthermore, several factors that contribute to the proper functioning of the insect immune system are highly conserved and perform analogous functions across evolution (HOFFMANN AND REICHHART 2002; LEMAITRE AND HOFFMANN 2007).

Interestingly, almost all the protein components of the insect immune system are highly pleiotropic and involve diverse activities during developmental progression. For example, the Toll class of proteins belonging to a larger family of pattern recognition receptors are essential while mounting robust immune response against the microorganismal invasion (BRENNAN AND ANDERSON 2004; WANG AND LIGOXYGAKIS 2006). The same proteins are also deployed earlier during embryonic patterning and morphogenesis (GOVIND 1999; HOFFMANN AND REICHHART 2002; VALANNE *et al.* 2011). Evidently, in several instances, different pathway components or modules used during early development are repurposed to mediate immunity both in the insect and the mammalian context (BELVIN AND ANDERSON 1996; GOVIND 1999; ROTH 2023).

The involvement of early embryonic morphogen, Dorsal, during humoral response in flies is a canonical example of the context-specific and diverse functions of immune system components (GOVIND 1999; ROTH 2023). Pathogenic invasion of insects induces both the humoral and cellular immune response (BELVIN AND ANDERSON 1996; WILLIAMS 2007). The humoral response consists of the production of antimicrobial peptides by the fat bodies, which serve as a first line of defence (BELVIN AND ANDERSON 1996; IMLER AND HOFFMANN 2000). Two Rel family member proteins, Dorsal and Dif, homologous to the mammalian NF-kappa B, induce the expression of defense peptides (BELVIN AND ANDERSON 1996; GOVIND 1999; BUCHON *et al.* 2014). NF-kappa B is essential for differentiating lymphocytes, which engineer the acute-phase response. Altogether, undertaking functional analysis of proteins, in a temporally distinct developmental context, has proven to be highly informative and insightful. Notably, however, thus far, such analysis has focused on only activator proteins. Here we have investigated the

99 embryonic function of Caspar (Casp), a protein involved in inhibiting the immune response (KIM
100 *et al.* 2006).
101 Casp is an intracellular negative regulator discovered in a genetic screen to identify
102 suppressors of antibacterial immunity (KIM *et al.* 2006). Flies mutant for *casp* were identified due
103 to their high rates of melanization, an innate immune response that leads to encapsulation of
104 pathogens in the gut and fat body. Interestingly, *casp* mutants isolated in this study were
105 resistant to Gram-negative bacterial infections due to elevated expression of the antimicrobial
106 peptide (AMP) diptericin; consequently, infected flies survived longer than their wild-type
107 counterparts. Strikingly, *casp* overexpression inhibited nuclear localization of Rel in response to
108 infection in the fat body. Excess levels of Casp result in the cytoplasmic retention of Rel in its
109 uncleaved, inactive form, presumably due to inhibition of the protease, Dredd (KIM *et al.* 2006).
110 Intriguingly, sequence analysis of Casp indicated a high degree of similarity to the
111 mammalian Fas-associated factor 1 (FAF1) protein (KIM *et al.* 2006; TENDULKAR *et al.* 2022)
112 (Fig.1A). FAF1 is evolutionarily conserved and was initially discovered as an interactor of Fas, a
113 pro-apoptotic member of the tumor necrosis factor receptor family (CHU *et al.* 1995). FAF1 also
114 interacts with the components of the death-inducing signaling complex (DISC) such as the Fas-
115 associated death domain (FADD) and Caspase-8 proteins (RYU *et al.* 2003). These interactions
116 are mediated by the death effector domains (DED) in FADD and Caspase-8 and the DED-
117 interacting domain (DEDID) in FAF1 (RYU *et al.* 2003). Both 'loss' and 'gain' of function
118 experiments indicated that FAF1 is crucial in promoting cell death via transduction of the
119 apoptotic signal (RYU AND KIM 2001; DE ZIO *et al.* 2008). FAF1, like its *Drosophila* ortholog, is a
120 negative regulator of NFκB signalling (MIN-YOUNG *et al.* 2004; PARK *et al.* 2007). FAF1's myriad
121 cellular functions can be attributed to its multiple protein-interaction domains that allow its
122 participation in ubiquitin-related processes such as protein degradation (SONG *et al.* 2005;
123 MENGES *et al.* 2009; ZHANG *et al.* 2011). Consistently, FAF1 harbors a Ubiquitin-associated
124 (UBA) domain, a UAS domain and a Ubiquitin-like regulatory X (UBX) domain (Fig. 1A).
125 Furthermore, the N-terminal UBA domain recruits polyubiquitinated proteins, leading to their
126 accumulation (SONG *et al.* 2009). The C-terminal UBX domain, on the other hand, interacts with
127 the molecular chaperone, valosin-containing protein (VCP/p97) bound to the Npl4-Ufd1
128 heterodimeric complex (SCHUBERTH AND BUCHBERGER 2008; KLOPPSTECK *et al.* 2012; EWENS *et*
129 *al.* 2014). FAF1 complexed with VCP-Npl4-Ufd1 and polyubiquitinated proteins is known to
130 assist endoplasmic reticulum-associated degradation (ERAD) (LEE *et al.* 2013). The UAS
131 domain, a domain of unknown function, is involved in interaction with long-chain fatty acids,
132 which is thought to promote the polymerization of FAF1 (KIM *et al.* 2013).

While Casp has a well-established role in the immune response, modENCODE RNAseq and proteomics data suggest that *casp* is also highly expressed in the 0-3 hour old embryo (BROWN *et al.* 2014; CASAS-VILA *et al.* 2017). Consistently, a snapshot of *casp* staining in a high-throughput RNA *in-situ* experiment indicates ubiquitous expression of maternally deposited *casp* in the *Drosophila* embryo (WEISZMANN *et al.* 2009). We thus wondered if Casp expression in early embryos is functionally relevant for proper developmental progression. To explore the possible developmental function of Casp, we first assessed if Casp function is needed for viability. Analysis of a hypomorphic allele of *casp* demonstrated that Casp is indeed required maternally for embryonic development. Consequently, roughly half of the embryos maternally compromised in *casp*, fail to undergo gastrulation. Furthermore, such embryos display developmental defects including aberrant cytoskeletal network starting from early blastoderm stages. Interestingly, Casp is expressed strongly in primordial germ cells (PGCs). Consistent with the enrichment, maternal reduction of *casp* significantly affects the total number of pole cells. Here, we present an analysis of *casp* function during early embryonic development and its role in the formation and/or specification of PGCs. We show that Casp activity regulates Oskar levels and centrosome function, two critical determinants of PGC fate in *Drosophila* embryo. Upon loss of *casp*, the total amount of Oskar and Smaug changed reciprocally to influence the PGC count. Ubiquitin-based protein degradation is critically involved during early embryonic events, including the maternal-zygotic transition. We present a model explaining the involvement of Casp and its protein partner, TER94, during germ cell development, considering their influence on the clearance of Smaug, a critical regulator of maternal to zygotic transition (MZT).

Results

Casp^{c04227} is a loss of function allele of casp.

To better understand embryonic function of Casp we decided to first characterize a *casp* allele, *w^{1118}; pBac(PB)casp^{c04227}* (Bloomington stock number:11373) (Supplementary Fig. 1A; labelled as S1A). This allele is induced by a piggyBac insertion in the 5' regulatory region of *CG8400/FBgn0034068/Casp* locus which is situated at 2R, region 52D14-15 (THIBAULT *et al.* 2004). As summarized in Fig. 1, our data indicate that *casp^{c04227}* is a strong hypomorphic allele and is referred to as a 'loss of function' allele (*casp^{lof}*) here onwards.

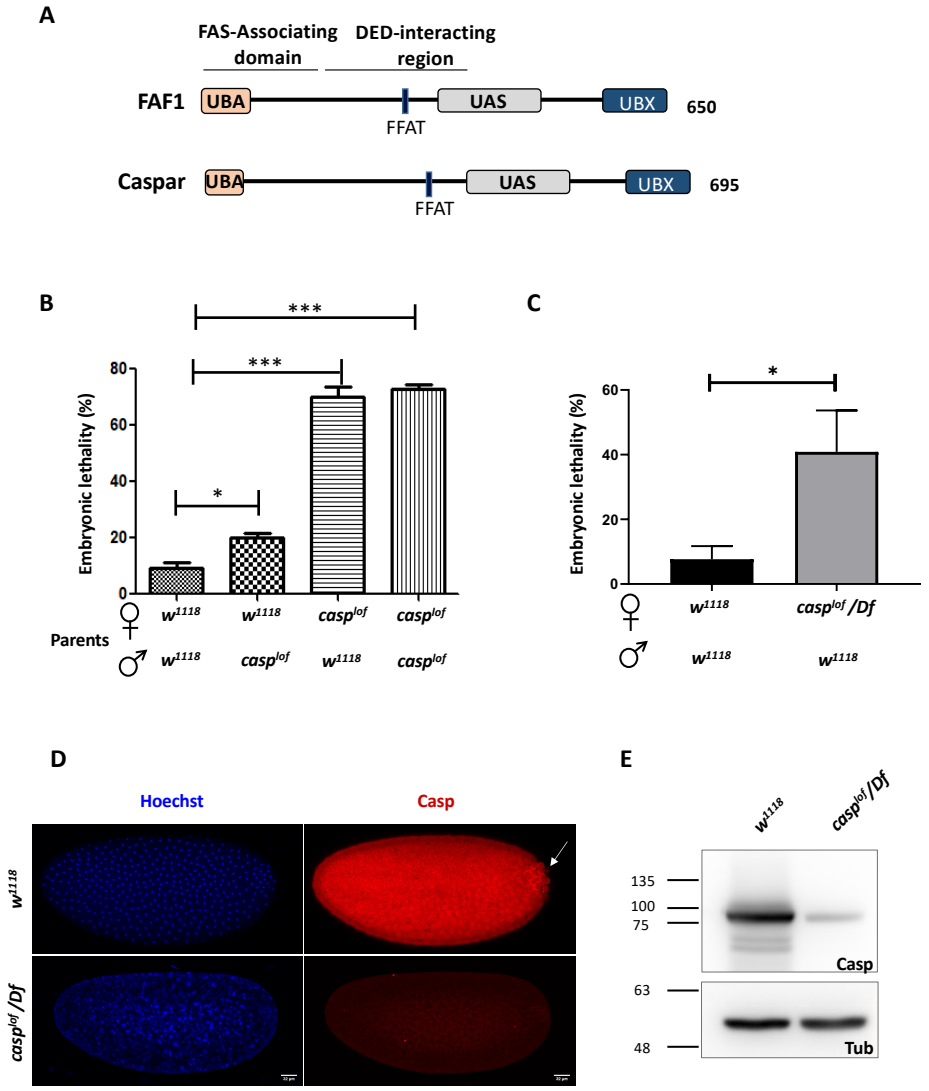

Fig. 1. *casp* is a maternal effect gene. (A) Comparison between human FAF1 and Casp shows conserved protein domains, which are described in the text. (**B**) Embryos laid by homozygous *casp^{lof}* females show ~70% lethality, irrespective of the paternal genotype (*w^{1118}* or *casp^{lof}*), suggesting a strictly maternal function of *casp* (**C**) The use of a Deficiency in the *casp* locus validates the lethal phenotype associated with the mutation, which drops to ~40%. In

panels B and C, the parental genotype is listed on the X-axis, with percent embryonic lethality plotted as a bar graph. N = 3, ordinary one-way ANOVA/ unpaired t-test, (***) $P < 0.001$, (*) $P < 0.05$. (**D**) Immunofluorescence images of 0-3 h embryos derived from w^{1118} and $casp^{lof}/Df$ females, stained with Hoechst and Casp (**E**) Casp protein levels were assessed in 0-3 embryos laid by w^{1118} and $Casp^{lof}/Df$ animals, evaluated via western blotting. Tubulin is used as a loading control. N = 3.

casp^{lof} adults are only partially homozygous viable as ~70% embryos laid by the homozygous mutant females failed to hatch into larvae (Fig. 1B). Moreover, the number of embryos that failed to hatch did not change substantially when *casp*^{lof} virgin females were mated either with w^{1118} males or *casp*^{lof} males. That the extent of viability was independent of the paternal genotype established that *casp* is a maternal effect gene and its activity is required for viability (Fig. 1B). To rule out the possibility that the lethality was induced by non-specific background mutations, we procured multiple deficiency (Df) lines spanning the 52D locus and confirmed that *casp*^{lof}*/Df* mothers also displayed significant embryonic lethality (40%) (Fig. 1C). Lastly, as in the case of *casp*^{lof} females, *casp*^{lof} males are also semi-fertile which was assessed by mating the mutant males with w^{1118} virgin females (Fig. 1B).

To better understand the function of Casp, we first decided to analyze how *casp* RNA and Casp protein are expressed during embryogenesis. Consistent with the maternal effect lethality, modENCODE (MUERS 2011; CHEN *et al.* 2014) data suggests that *casp* mRNA is deposited maternally, being highly expressed in the 0-2 hours embryo, with a drop in expression 2-4 hours post fertilization (Fig. S1B)(BROWN *et al.* 2014). Publicly available *In-Situ* databases such as FlyAtlas, Fly-FISH and BDGP (WEISZMANN *et al.* 2009) (TOMANCAK *et al.* 2002; LECUYER *et al.* 2007) also confirmed maternal deposition of *casp* mRNA, with ubiquitous expression seen in stage 1-3 embryos (Fig. S1C). Fly-FISH data (LECUYER *et al.* 2007; WILK *et al.* 2016) further suggests that expression in the pole cells persists while maternally deposited somatic transcripts are selectively degraded from stage 4 onwards. We immunostained 0-3 hours old embryos derived from w^{1118} mothers with the anti-Casp antibody (TENDULKAR *et al.* 2022) and found that Casp protein was predominantly cytoplasmic, and as in the case of RNA, exhibited a relatively ubiquitous distribution in the somatic compartment (Fig. 1D). Again, consistent with the *in-situ* hybridization pattern, Casp-specific antibody staining appeared to be enriched in the posteriorly localized primordial germ cells (PGCs) compared to the surrounding soma (Fig. 1D, arrow). To establish the specificity of the anti-Casp antibodies in the embryonic context, we stained the embryos laid by both the *casp*^{lof}/ *casp*^{lof} and *casp*^{lof}/*Df* mothers. As expected, Casp protein was nearly absent in embryos of both these genotypes suggesting that Casp protein is significantly reduced in the 0-3 hours old *casp*^{lof} mutant embryos. Analysis of the embryonic lysates using Western blotting, suggested that trace amounts of Casp protein

241 (estimated 5-10% of w^{1118}), were present in embryos laid by $casp^{lof}/casp^{lof}$ and $casp^{lof}/Df$
242 mothers, supporting the conclusion that $casp^{lof}$ is a strong hypomorphic allele and not a null
243 (Fig.1E). Interestingly, mature egg chambers of wild-type animals had Casp expression in
244 somatically derived follicle cells, but Casp protein could not be readily detected in the egg itself
245 (Fig. S1D). This observation suggested that, unlike the RNA, only trace amounts of Casp
246 protein may be maternally deposited. Thus, the protein detected in the young embryos is likely
247 generated post-fertilization, by the translation of maternally deposited *casp* mRNA.
248
249 ***Casp function is required for early embryonic development.***
250 Larval cuticle patterns are an excellent readout for major patterning defects in
251 *Drosophila (NUSSLEIN-VOLHARD AND WIESCHAUS 1980)*. To better understand the function of
252 Casp protein during embryonic development, we analyzed the cuticles of *casp* mutant embryos.
253 0-3 hours old embryos laid by $casp^{lof}/Df$ mothers were collected and aged for 22 hours to
254 prepare cuticles (see Material and Methods). The cuticular patterns were visualized under a
255 dark field microscope. While ~60% of larvae displayed cuticular patterns comparable to wild
256 type larvae, development in the remaining 40% embryos appeared to have stalled before they
257 could deposit cuticle. These data were consistent with the extent of maternal effect lethality.
258 Next, to define the stage of developmental arrest, we performed time-lapse live Bright-field
259 imaging (CAVEY AND LECUIT 2008). These data (Movies, Fig. S2A) confirmed that 40% of
260 embryos did not proceed to gastrulation and showed developmental arrest before germ band
261 extension (around stage 6; Fig. S2, panels C4, D4). Such embryos displayed irregular,
262 uncoordinated morphogenetic movements with blebbing of the plasma membrane possibly
263 inhibiting both cephalic furrow formation, and germband elongation (Fig. S2 panels C2-C3, D2-
264 D3).
265
266 ***Compromising casp activity leads to centrosomal abnormalities in early embryos.*** To
267 trace the defects during mid-embryogenesis including failure of gastrulation, we sought to
268 visualize $casp^{lof}$ embryos at blastoderm stage. We labelled the 0-3 hours old $casp^{lof}$ and control
269 embryos with the nuclear dye Hoechst and the cytoskeletal F-actin marker phalloidin (Fig. 2A,
270 B). $casp^{lof}$ embryos displayed significant structural abnormalities that are reflected in an irregular
271 actin network that lacks stereotypical organization, which is partially interrupted in several
272 places (Fig. 2B1, compared to Fig. 2A1). Similarly, unlike the age-matched control embryos,
273 regular nuclear spacing is disrupted, and nuclei are unevenly distributed across the embryo with
274 occasional instances of nuclear fusion and possibly mitotic asynchrony (Fig. 2B vs Fig. 2A).

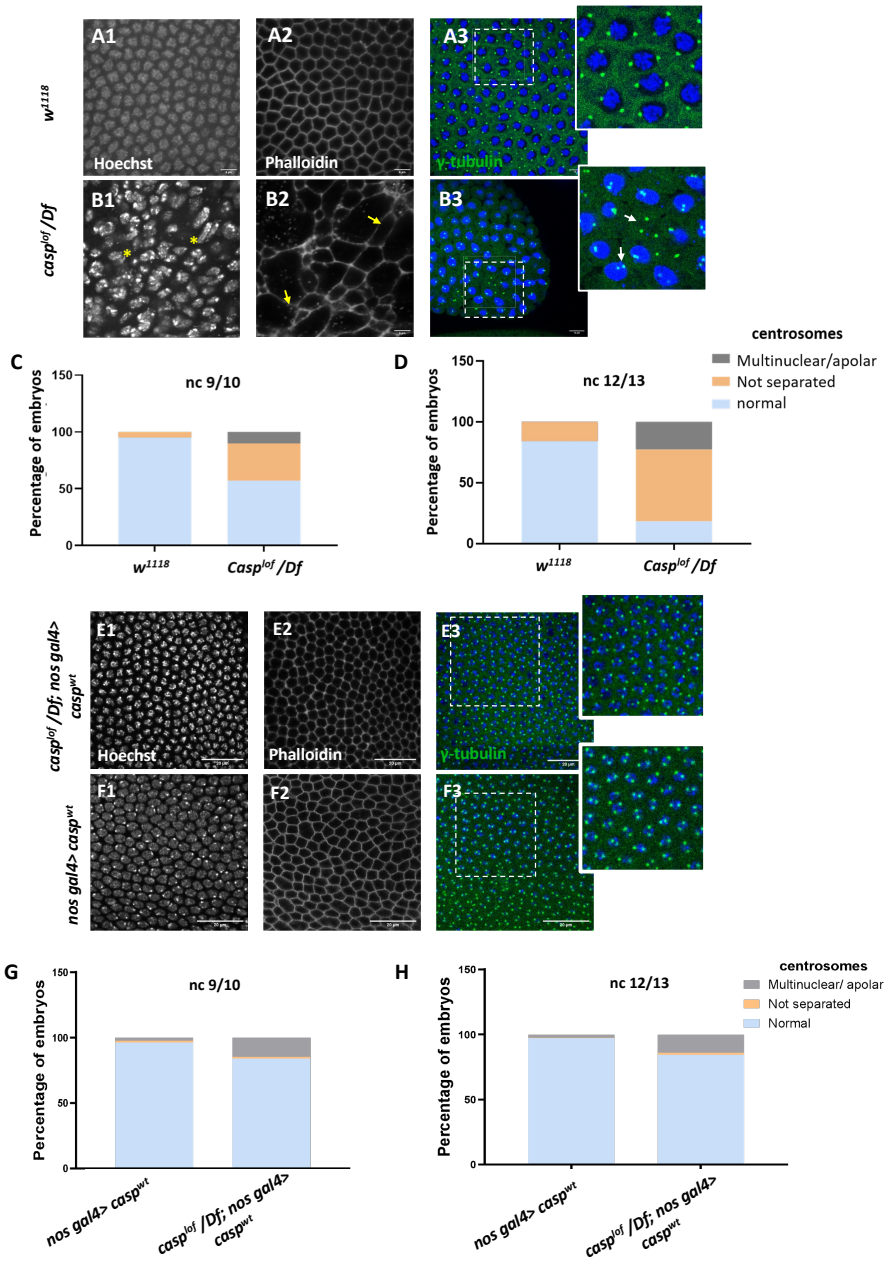

Fig. 2. A Significant proportion of embryos (~45%) laid by *casp^{lof}/Df* mothers display nuclear division and cytoskeletal defects. (**A-B**) Confocal images of nuclear cycle 13/14 embryos (single sections) of the indicated genotypes stained with Hoechst, phalloidin, and gamma-tubulin. Both the regular arrangement and uniform density of nuclei are disrupted in the mutants, as indicated by a yellow asterisk. F-actin, marked with phalloidin, shows a regular, hexagonal compartmentalization in *w^{1118}* (panel A2), while disorganized F-actin (white arrows; panel B3) is observed in the mutant. Defective centrosomes marked with gamma-tubulin can also be observed in the *Casp* mutant (inset of B3, compare to inset A3), indicated by yellow arrows. The extent of defects is quantified in nuclear cycle(nc) 9/10 (**C**) and nc 12/13 (**D**). (**E-F**) Confocal images of sections of nc 13/14 embryos of the indicated genotypes stained with Hoechst, phalloidin, and gamma-tubulin. The nuclear, cytoskeletal, and centrosomal defects are rescued (panel E) when wild-type *casp* is expressed in the *casp^{lof}/Df* background (compare panels **G-H** to C-D). Overexpression of *casp* on its own (panel F) does not appear to affect nuclear or cytoskeletal architecture. The bar charts represent the percentage of defective centrosomes in nuclear cycle 9/10 and 12/13 embryos. N = 15.

328 The nuclear and cytoskeletal defects observed in *casp* embryos prompted us to analyze
329 the centrosomes in embryos deficient in *casp* function. Centrosomes function as the microtubule
330 organizing centers, and actomyosin-based cytoskeletal defects have been correlated with
331 aberrant centrosome activity. In wild-type nuclei, centrosome duplication occurs simultaneously
332 with the initiation of the nuclear division cycle. After completion of duplication, centrosomes
333 separate and migrate along the nuclear membrane to reach the opposite sides of the nucleus
334 (reviewed by (LATTAO *et al.* 2017; WU AND AKHMANOVA 2017; BLAKE-HEDGES AND MEGRAW
335 2019)). In the embryos maternally compromised for *casp*, several characteristic aspects of
336 centrosome behavior during mitotic divisions are altered (Compare Fig. 2B3 to Fig. 2A3). At
337 times, centrosomes appeared to divide even without a nucleus (or DNA), and many 'orphan'
338 centrosomes devoid of nuclear DNA were observed (Fig. 2B3, inset). By contrast, in some
339 instances, centrosomes were duplicated but remained in proximity indicating failed or
340 incomplete migration (see arrows in Figure 2B3, inset). Quantitation of the centrosomal
341 abnormalities in $casp^{lof}$ embryos (Fig. 2C, D) further revealed that the behavior of the
342 centrosomes, especially their ability to separate and migrate to the opposite poles correctly
343 deteriorated progressively (Compare Fig. 2D to Fig. 2C), as nuclear division cycles advanced.
344 To confirm the specificity of the phenotypic consequences induced by the maternal loss
345 of *casp*, we overexpressed *UAS-*$casp^{wt}$ transgene in $casp^{lof}$*/Df* embryos using *nos Gal4*, a
346 maternal Gal4 driver. Embryos derived from such mothers were stained using nuclear dye
347 Hoechst, phalloidin and anti-Gamma tubulin antibodies that mark the centrosomes. As shown in
348 Fig. 2E, maternal overexpression of *casp* substantially rescues centrosomal and cytoskeletal
349 abnormalities seen in $casp^{lof}$ (compare panels E1-E3 to A1-A3). This rescue is quantitated in
350 Fig. 2 G, H (compare with Fig. 2C, D). The $casp^{lof}$*/Df; nos Gal4/UASp-*$casp^{wt}$ showed a rescue
351 of lethality of 20-25% as compared to 40-45% for $casp^{lof}$*/Df*.
352 Taken together, these data showed that Casp plays an essential role in early embryonic
353 development in *Drosophila*, and loss of <u>*casp*</u> results in conspicuous nuclear and cytoskeletal
354 defects that correlate with incomplete gastrulation movements and developmental arrest, for
355 ~45% of embryos. Moreover, such defects do not appear to be region-specific or localized
356 within an embryo arguing in support of ubiquitous function across the embryo for Casp protein.
357
358

359 ***Maternal Casp protein is enriched in pole cells and controls total pole cell count in***
360 ***blastoderm embryos.***
361 As the early syncytial nuclear division cycles progress, a few nuclei and centrosomes
362 associated with them invade posteriorly localized and anchored pole plasm ahead of the rest of
363 the somatic nuclei (RAFF AND GLOVER 1989). The precocious entry of the centrosomes results in
364 the release and microtubule-dependent transport of pole plasm, which is sequestered in newly
365 cellularized PGCs (RAFF AND GLOVER 1989; LERIT *et al.* 2017). Thus, the PGCs or the germline
366 stem cell precursors are set aside during early embryogenesis. Moreover, centrosome behavior
367 and dynamics are crucial for proper cellularization and mitotic cell divisions of early germ cells
368 (LERIT AND GAVIS 2011; LERIT *et al.* 2017). Centrosomes, the microtubule (MT)-organizing
369 centers, ensure the faithful segregation of germ plasm, a reservoir of germ cell determinants,
370 into PGCs. Taken together with the observation that Casp protein is readily detectable in early
371 PGCs, we wondered if it could influence the total pole cell count. To examine this possibility,
372 stage 5 embryos derived from *cs* and $casp^{lof}$/ *Df* mothers were immunostained for the pole cell
373 marker Vasa and visualized under a confocal fluorescence microscope. Interestingly, while *cs*
374 and *nos-Gal4* embryos had an average of ~30 pole cells (Fig 3, panels A1-B3, for quantitation
375 see panel F) $casp^{lof}$/ *Df* showed a drastic reduction in total PGC count to ~10 (Fig. 3 panels C1-
376 3, F). By contrast, stage 5 embryos derived from *nosGal4>UAS-casp* mothers, where *casp* was
377 overexpressed (Fig. 3G), displayed considerably elevated total number of PGCs (Fig. 3, panels
378 E1-E3, F). To confirm that the loss of *casp* is specifically responsible for the reduction in the
379 total number of PGCs, we simultaneously overexpressed *casp* in the $casp^{lof}$/*Df* mothers in a
380 germline-specific manner, which resulted in a significant rescue (~26 pole cells; Fig.3, panels
381 D1-D3, F). Taken together, these data suggested that the total pole cell number in late syncytial
382 /cellular blastoderm embryos specifically depends on *casp* function. Furthermore, increasing
383 *casp* levels maternally, is sufficient to elevate the total pole cell number substantially.
384
385
386
387

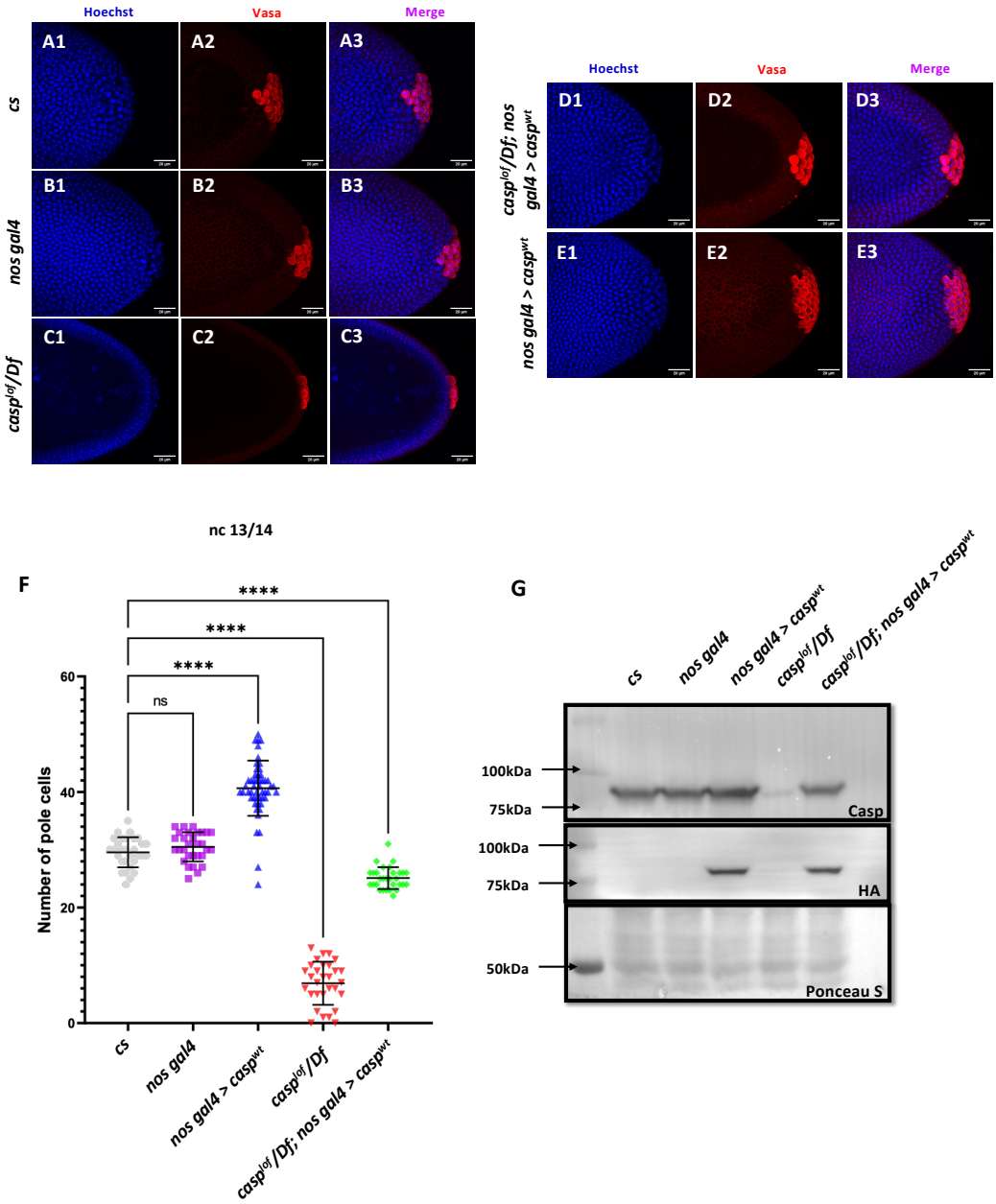

Fig. 3. Casp influences total PGC count. (**A-E**): Shown are the Confocal images of the posterior terminii of nuclear cycle 13/14 embryos of the following genotypes: *cs* (A1-A3), *nos gal4* (B1-B3), *casp*^{lof}*/Df* (C1-C3), casp^{lof}*/Df*; *nos gal4>casp*^{wt} (D1-D3) and *nos gal4> casp*^{wt} (E1-E3). Embryos were immunostained with Vasa (1:50) antibody. Hoechst marks the nuclei. (**F**) The total number of germ cells marked with Vasa were quantified and plotted as bar graphs. N (embryos)= 30. Ordinary one-way ANOVA, (****) P <0.0001. (**G**) Casp protein levels were assessed in 0-3 embryos via western blotting. Rabbit anti-Casp (1:10,000) and rabbit anti-HA (1:2000) antibodies were used to probe the blot. Ponceau is used as a loading control. N = 3.

Casp interacts with TER94 in the early embryo.

Data presented in the previous section demonstrated that both the 'loss' and 'gain' of *casp* activity exert reciprocal influence on total PGC numbers in early embryos. As very few germ

442 plasm components have been shown to display this trait (JONGENS *et al.* 1994), we decided to
443 explore the phenomenon further. We have previously reported that Casp protein physically
444 associates with both transitional endoplasmic reticulum ATPase (TER94; also called valosin-
445 containing protein, VCP or p97) and vesicle-associated membrane protein-associated protein B
446 (VAPB/VAP33A)(TENDULKAR *et al.* 2022). Furthermore, based on interaction studies and
447 biochemical analysis, we proposed that Casp may act as an adapter that either directly or
448 indirectly mediates the physical association between VAPB and TER94 (TENDULKAR *et al.*
449 2022). To arrive at this conclusion, we had primarily relied on S2 cell lysates as well as adult
450 and fly head total protein extracts. To specifically identify the major protein partners of Casp in
451 the early embryos, we performed similar immunoprecipitations using anti-Casp antiserum in
452 early (0-3 hour) embryonic lysates and interactors were identified via mass spectrometry (Fig.
453 S3A). Peptides from 122 proteins were recovered in the Casp IP but not the IgG IP and thus,
454 were considered significant interactors. The top 23 interactors are presented in Fig. S3A**.**
455 Interestingly, as in the case of brain and S2 cell lysates, TER94 and VAPB were the top hits,
456 with germ cell determinants also identified as interactors (Fig. S3C; Discussed in a subsequent
457 section). These observations suggested that a functional protein complex between Casp,
458 TER94 and VAPB likely exists in many different tissue/cellular contexts, including early
459 embryos**.**
460
461 ***Maternal requirement of TER94.***
462 Mammalian VCP/p97 is an essential chaperone for proteostasis that modulates several
463 ubiquitin-associated processes (PETERS *et al.* 1990; DAI *et al.* 1998; MEYER *et al.* 2000; MEYER
464 2005; YE 2006; JENTSCH AND RUMPF 2007; MEYER *et al.* 2012). Its *Drosophila* counterpart
465 TER94 has been studied mostly in the context of neurodegeneration (GRICIUC *et al.* 2010;
466 CHANG *et al.* 2011; AZUMA *et al.* 2014; KUSHIMURA *et al.* 2018; TENDULKAR *et al.* 2022;
467 THULASIDHARAN *et al.* 2024). Loss of TER94 was shown to ameliorate polyQ-induced eye
468 degeneration. Moreover, the overexpression of TER94 promoted the apoptosis of neuronal cells
469 (HIGASHIYAMA *et al.* 2002).
470 TER94 is one of the significant interactors of Casp protein in the embryonic context as
471 suggested by the Casp interactome (Fig. S3A) and has been implicated in ER-associated
472 degradation (CHANG *et al.* 2011; TENDULKAR *et al.* 2022). Thus, we wondered if TER94 also has
473 a maternal function and whether embryos maternally compromised for *TER94* display similar
474 phenotypes as *casp*. To achieve this, we employed VALIUM 20/22 maternal RNAi lines (*UAS*-

TER94i). First, we used a *mat-α4tubulin:VP16-Gal4* (*Mat-αtubGal4*) driver to deplete *TER94* activity in the late stages of oogenesis (Fig. 4).

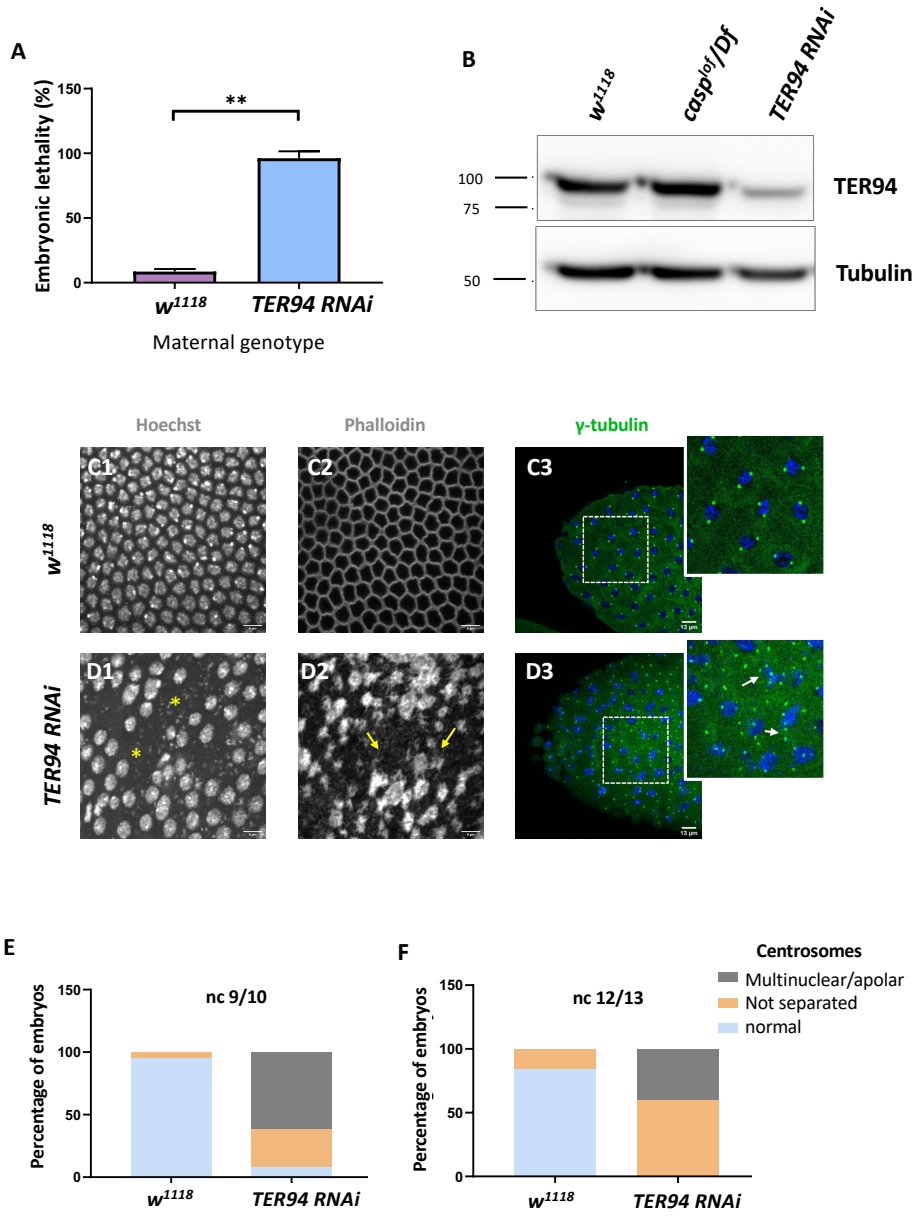

Fig. 4. Maternal requirement of *TER94* during early embryogenesis. (**A**) Viability of embryos derived from w^{1118} and *Mat-αtubGAL4 > TER94i* (referred to as *TER94 RNAi* henceforth) mothers is represented as a bar graph. N = 3, ordinary one-way ANOVA, (***) P <0.001. (**B**) Western blot analysis indicates the knockdown efficiency of TER94 in the 0-3 h embryo, estimated to be ~90%. TER94 levels remain unaffected in $casp^{lof}/Df$ embryos. Tubulin was used as a loading control. N = 3. (**C, D**) Confocal images of sections of nuclear cycle 13/14 embryos of the indicated genotypes stained with Hoechst, phalloidin, and gamma-tubulin. Nuclei and F-actin are visualized with Hoechst and phalloidin respectively. Nuclear disruption (D, asterisks) and F-actin aggregates (D2, arrows) are observed in the mutant. Defective centrosomes (D3, arrows, inset) can be observed in the *TER94 RNAi* embryos. (**E, F**) The percentage of defective centrosomes in nuclear cycles 9/10 and 12/13 are represented as bar charts. n = 10.

529 We sought to observe the consequence of *TER94* knockdown both in the adult females
530 and early embryos derived from such females. In the females compromised for *TER94*, egg-
531 laying behavior remained largely unaffected. Interestingly, however, the viability of such
532 embryos was severely impaired, with >95% of embryos failing to hatch (Fig 4A).
533 A western blot of lysates derived from *Mat-GAL4>UAS-TER94i* mothers probed with
534 anti-TER94 antiserum indicated a robust knockdown of TER94 as compared to control (Fig. 4B).
535 Phenotypic analysis of embryos derived from *Mat-GAL4> TER94i* females revealed that >70%
536 of *Mat-GAL4/ TER94i* embryos failed to progress to the syncytial blastoderm stage, with even
537 fewer reaching Stage 5. The late-stage syncytial/ cellular blastoderm embryos were further
538 assessed for cell cycle defects. As in the case of $casp^{lof}/Df$, *Mat-GAL4>TER94i* embryos also
539 displayed defects ranging from irregular nuclear distribution to perturbed F-actin localization, as
540 assessed by HOECHST and phalloidin staining, respectively (Compare Fig. 4D1-D3 with Fig.
541 4C1-C3).
542 We also examined if maternal loss of *TER94* activity results in centrosome aberrations
543 like those observed in $casp^{lof}$ embryos. Indeed, embryos deficient in *TER94* function showed
544 both the characteristic phenotypes observed in the *casp* embryos including a) inefficient
545 separation of duplicated centrosomes and b) multiple instances of 'orphan' centrosomes devoid
546 of nuclear DNA (Fig. 4E, F).
547 Taken together, these data demonstrated that embryos maternally compromised for
548 either Casp or TER94 functions share several phenotypes, suggesting that both the proteins
549 likely perform essential and likely related functions during syncytial nuclear cycles in *Drosophila*
550 embryos. Furthermore, the phenotypic consequences observed upon maternally compromising
551 *casp* and *TER94* overlap but are not identical, with TER94 embryos showing higher penetrance
552 in terms of phenotypes and embryonic lethality. Future experiments will be necessary to resolve
553 the functional distinction between the two.
554
555 ***TER94, a known component of pole plasm, is detectible in PGCs.***
556 Maternal loss of TER94 function mimicked both the cytoskeletal and corresponding
557 centrosome aberrations observed upon similar loss of *casp* activity. Both centrosomes and
558 germ plasm, are essential for the proper specification and formation of PGCs in *Drosophila*
559 embryos (LERIT AND GAVIS 2011; LERIT *et al.* 2017). This prompted us to examine the Casp
560 interactome for the possible enrichment of germ plasm components and proteins that may
561 regulate centrosome dynamics and/or behavior. Fig. S3B lists Casp interactors that are

562 important constituents of the germplasm, including eIF4A, me31B, and TER94, known
563 constituents of the polar granules (THOMSON *et al.* 2008).
564 Among the different components of the germ plasm, Oskar serves as the master
565 determinant of the PGC fate (KIM-HA *et al.* 1991; SNEE AND MACDONALD 2004; VANZO *et al.*
566 2007; LEHMANN 2016). Supporting the conclusion, the loss and gain of function of *oskar* leads to
567 reciprocal phenotypes. Compromising *oskar* activity maternally, leads to reduction in total
568 number of PGCs whereas anterior ectopic expression of *oskar* using the *bicoid* mRNA
569 localization signal induces pole cell formation at the anterior (EPHRUSSI AND LEHMANN 1992).
570 The germ plasm is supplemented with mitochondria and polar granules, which consist of
571 ribonucleoprotein complexes. Downstream of *oskar*, *vasa* and *tudor* are two genes that are
572 essential for the assembly of pole plasm (BREITWIESER *et al.* 1996; ARKOV *et al.* 2006; JONES
573 AND MACDONALD 2007). Biochemical proteomic analysis of Vasa (VAS) and Tudor (TUD)
574 containing polar granule complexes identified eIF4A, me31B, and TER94. This indicated that
575 the germ plasm consists of the components of translational machinery and the endoplasmic
576 reticulum assembly (THOMSON *et al.* 2008).
577 TER94 is a component of pole plasm and is also physically associated with Casp.
578 Furthermore, proteomic analysis indicated that Casp could be part of a complex comprising
579 several germ plasm proteins including Tudor and Me31B. To confirm that, as in the case of
580 Casp, TER94 is also detected in PGCs. We used antibodies generated against Casp (Fig. S3D)
581 and TER94 (Fig. S3E) to label wild-type embryos. Embryos were also co-immunostained for
582 germ cell specific marker, Vasa. As can be seen, both Casp and TER94 proteins are found in
583 PGCs, colocalized with Vasa.
584
585 ***Casp and TER94 regulate embryonic germ cell formation*.**
586 As we were specifically interested in investigating possible similarities and distinctions
587 between the respective functions of TER94 and Casp during early embryonic germ cell
588 development, we decided to examine their possible functions during PGC formation (also
589 referred to as pole cell budding). This seemed especially pertinent as centrosome behavior and
590 dynamics are crucial for proper formation and cellularization of PGCs. Evidently, a germ plasm
591 component, Germ-cell-less (Gcl) was shown to be necessary for proper separation of daughter
592 centrosomes in the dividing pole buds (LERIT *et al.* 2017). Similarly, loss of centrosome
593 components such as Centrosomin results in partial loss of early embryonic PGCs. As maternal
594 loss of both *casp* and *TER94* results in aberrant centrosomes in the surrounding somatic nuclei
595 in early blastoderm embryos, we sought to investigate if posteriorly positioned centrosomes in

596 the vicinity of pole plasm also display similar problems. Indeed, maternally compromising *casp*
597 led to significant loss of pole buds and corresponding defective centrosome behavior (Fig.5).
598
599
600

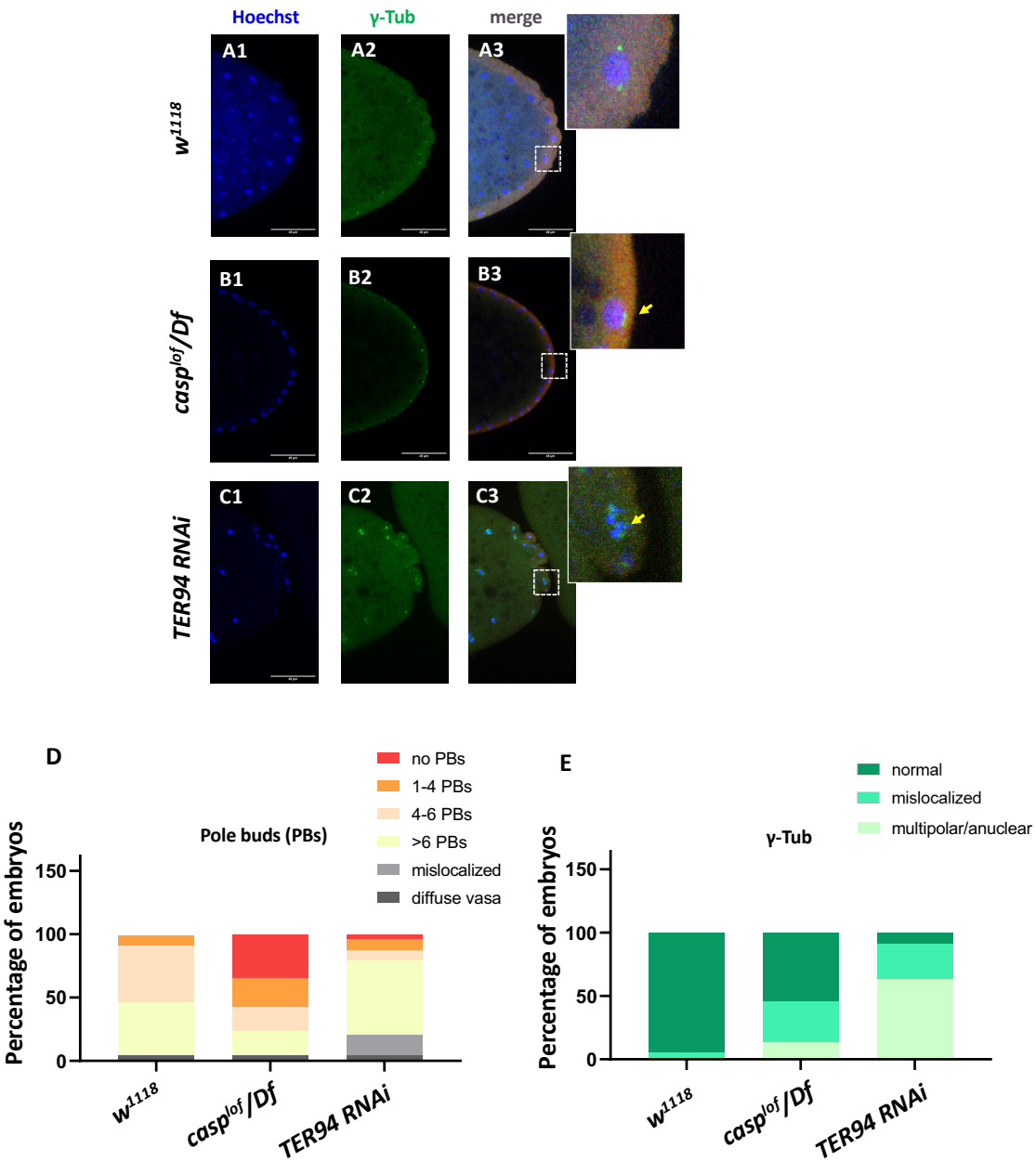

601
602 **Fig. 5. *casp and TER94* regulate pole bud formation. (A-C)** Confocal sections of the posterior termini of nuclear
603 cycle 9/10 embryos derived from w^{1118} (A1-A3), $casp^{lof}/Df$ (B1-B3), and *TER94 RNAi* (C1-C3) mothers
604 immunostained with gamma-tubulin. γ-tubulin labels centrosomes of pole buds, identified based on Vasa staining.
605 Nuclei are stained with Hoechst. The inset(s) for B3 and C3 highlight the centrosomal defects (arrow) when
606 compared with A3. Defects were quantified and plotted as bar graphs in (**D**) and (**E**) respectively. n = 20.
607

608 Especially these pole buds display defective centrosome separation and/or orphan
609 centrosomes (Fig. 5B1-B2,D,E), as observed in the somatic nuclei. Intriguingly, while *casp*^{lof}
610 embryos show discernible loss of pole buds, *TER94i* embryos displayed an increased number
611 of round-shaped, 'bud-like' cells at the posterior of the stage 3 embryos (Fig 5 C1-C2). Typically,
612 such ectopically localized pole buds also showed inadequate separation of centrosomes and
613 could be identified as pole buds due to the enrichment of Vasa. However, Vasa distribution and
614 accumulation in *TER94i* buds was variable and non-uniform. Since TER94 is required for *Osk*
615 mRNA localization in the oocyte, the defects in pole cell budding including their ectopic
616 positioning could be a consequence of inappropriate segregation of *oskar.* Moreover, the early
617 nuclear division cycles and nuclear migration defects seen in are defective in *TER94i* embryos
618 could also contribute to PGC formation/ cellularization. Notably, although the pole bud count is
619 elevated in *TER94i* embryos, presumably, these pole buds don't survive through subsequent
620 nuclear cycles, and consequently, late blastoderm *TER94i* embryos almost completely lack
621 PGCs.

622 ***Casp activity is needed for the accumulation of Oskar protein at the embryonic***
623 ***posterior pole.***

624 Taken together, our data demonstrate that change in Casp levels leads to corresponding
625 alteration in the total PGC count. Moreover, PGC formation is affected by maternal loss of
626 Casp, although the precise nature of its involvement in this process remains to be determined.
627 As Oskar is the master determinant of germ cell fate, we sought to determine if Oskar levels
628 (KIM-HA *et al.* 1991; EPHRUSSI AND LEHMANN 1992) are correspondingly altered upon change in
629 Casp. To assess this possibility, we stained wild-type control embryos and embryos maternally
630 compromised for *casp* using anti-Oskar antibodies (Compare Fig 6B to 6A). Simultaneously, we
631 stained embryos derived from *nosGal4>UASp-casp* mothers (Fig 6C1-C3) that display
632 significantly elevated number of PGCs, presumably due to excess levels of Casp protein in the
633 germline.

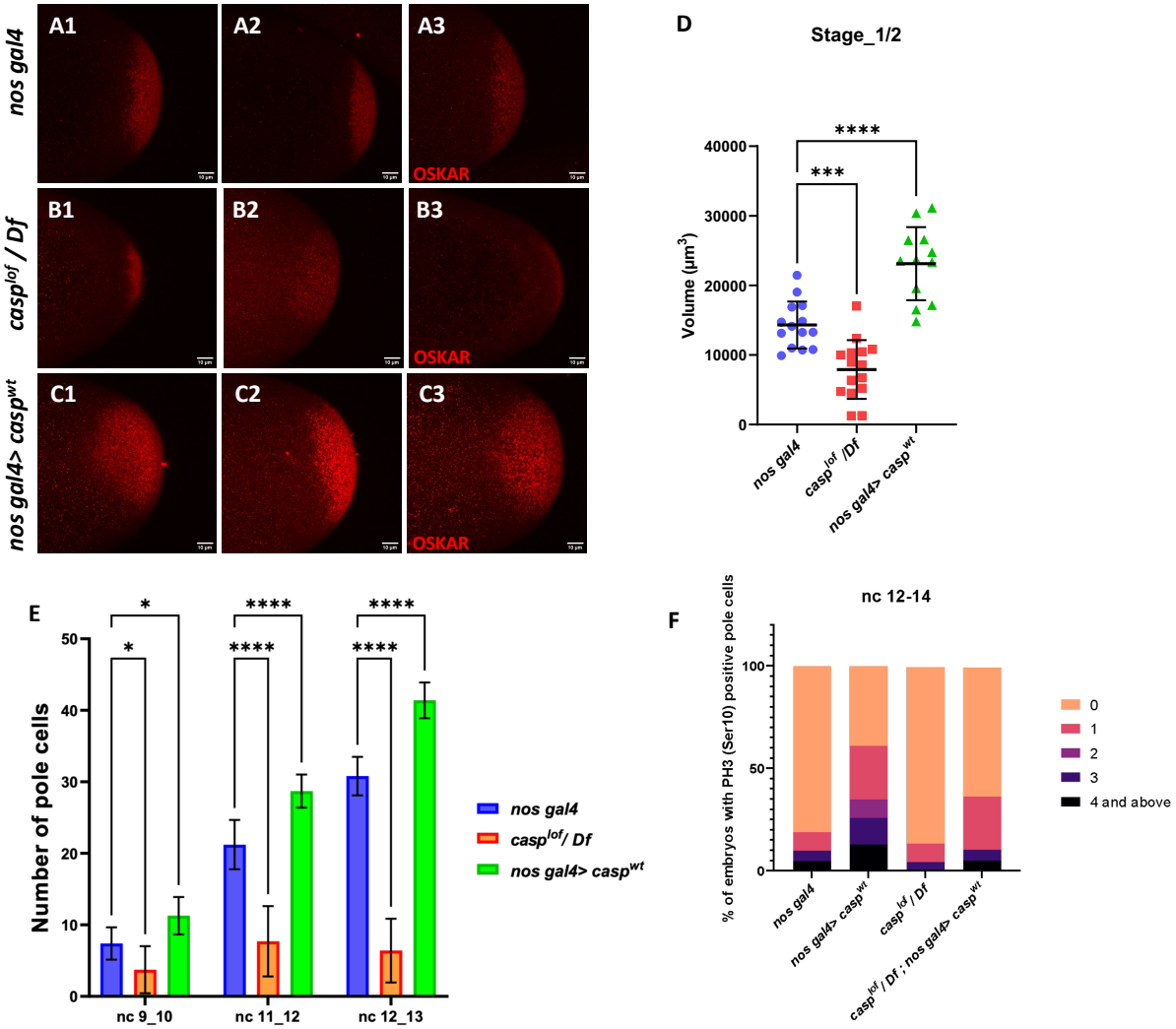

Fig. 6. Casp regulates Oskar levels and modulates cell division
(A-C) Confocal microscopy images of stage 1/2 embryo laid by w^{1118}, *casp*^{lof}*/Df*, and *nos gal4> casp*^{wt} females and immunostained with Oskar antibodies. Replicate (1-3) are shown to highlight variable reduction in Oskar levels. In addition, as compared to controls (w^{1118}) embryos (A1-A3), spread of Oskar appears to be restricted in *casp*^{lof}*/Df* (B1-B3) whereas it is expanded in *nos gal4> casp*^{wt} (C1-C3).
(D) Volume occupied by Oskar, per embryo is measured and plotted for all three genotypes (w^{1118}, *casp*^{lof}*/Df*, and *nos gal4> casp*^{wt}), n = 8. Ordinary one-way ANOVA, (**) P <0.01, (*) P *<0.05*.
(E) Number of pole buds (nc 9/10) and pole cells (nc 11/12, nc 12/13) in 0-3h old *nos gal4, casp*^{lof}*/Df and nos gal4> casp*^{wt} embryos at different nuclear cycles. Two-way ANOVA, (*) P <0.05, (****) P <0.0001. n = 10
(F) Graph showing the distribution of actively dividing pole cells as indicated by the presence of phospho-histone 3 (Ser10) antibody. Quantitative analysis was performed using nuclear cycle 12-14 in 0-3h old, *nos gal4*, *casp*^{lof}*/Df*, *nos gal4> casp*^{WT} and *casp*^{lof}*/Df;nos gal4> casp*^{WT} embryos.

Satisfyingly, the change in Oskar protein levels is consistent with the alteration in the Casp levels in the maternal germline (Fig 6D). Embryos derived from *casp* mutant mothers show considerably diminished levels of Oskar as compared to the control whereas overexpression of Casp in the maternal germline results in elevation in the Oskar protein amount (Fig 6D).

652 Furthermore, in all instances, Oskar protein appears to be anchored to the posterior pole as the
653 wild-type control embryos and the only discernible change is observed in its levels.
654
655 ***Casp levels influence total number of phosphor-histone3 (pH3) positive pole buds and***
656 ***PGCs.***
657 Changes in Casp protein levels influence the accumulation of Oskar protein. Oskar is
658 necessary and sufficient to assemble pole plasm at the posterior pole which controls the total
659 number of pole buds in an embryo. To directly evaluate the influence of Casp on pole bud
660 formation, total number of pole buds and pole cells were quantitated upon maternal loss and
661 gain of Casp against the control embryos at the same stage (Fig. 6E). Consistent with the data
662 presented in the previous sections, total number of pole buds (nc 9 and 10) were reduced in
663 *casp^{lof}* embryos whereas the number was elevated in the presence of excess Casp (Fig 6E).
664 Similar quantitation was performed in older embryos in two stages (nc11-12 and NC12-13), and
665 a progressive increase was observed in the total number of PGCs upon the gain of Casp
666 function (Fig. 6E). By contrast, the total PGC count for *casp^{lof}/Df* embryos did not increase
667 appreciably at nc11-12 and nc12-13.
668 Primordial germ cell number is determined by limited mitotic cell divisions that each pole
669 bud undergoes in a stochastic and asynchronous manner. As these are mitotic divisions, the
670 dividing PGCs can be identified using antibodies against the miotic marker phosphoHistone3
671 (pH3). As the total number of pole buds and PGCs change per Casp levels, we wanted to
672 examine if this is also reflected in the total number of pH3-positive germ cells simultaneously
673 labeled with the anti-Vasa antibodies. We decided to focus on syncytial blastoderm embryos
674 between NC12-14. As anticipated, maternal overexpression of Casp led to a corresponding
675 increase. In control (*nos gal4*) embryos, roughly 20% PGCs display either 1 or >1 pH3 positive
676 PGCs whereas, 70% of *nos-gal4>Casp^{WT}* embryos show 1 or >1 pH3 positive PGCs (Fig. 6F).
677 Conversely, less than 10% of *casp^{lof}* embryos showed either 1 or >1 pH3 positive PGCs and
678 pole cells with 3 or >3 pH3 positive cells were completely absent in this background as opposed
679 to 25% present in the control embryos (Fig. 6F). Importantly, maternal expression of the rescue
680 construct in the *casp^{lof}* embryos ameliorated the loss of pH3 positive PGCs seen in just the
681 mutant (*casp^{lof}*) PGCs.
682
683
684
685

686 ***Does Casp function affect canonical MBT regulators?***

687 Our analysis thus far has revealed two related yet distinct phenotypes associated with
688 maternal loss of *casp*. First, it can influence proper PGC formation and specification during
689 early embryonic development via its effect on the accumulation of germ cell determinant, Oskar.
690 Subsequently, it helps orchestrate cellular movements leading up to gastrulation during mid-
691 embryogenesis. While the first activity is likely germ cell autonomous, the second relates to its
692 role in the somatic cells/nuclei. Moreover, both the somatic and germline compartments of
693 *casp*^{lof} embryos share centrosomal as well as cytoskeletal aberrations. We thus wondered
694 whether the two activities are mechanistically connected, and if the possible connection relates
695 to the maternal-to-zygotic transition (MZT). One aspect of the MZT that has been highlighted in
696 recent years is the active degradation of maternal proteins (CAO *et al.* 2020). These proteins
697 comprise 2% of the maternal proteome and are degraded abruptly, at the end of the MZT. In
698 *Drosophila*, ubiquitin-proteasome-based degradation of three repressor proteins, namely Smaug
699 (Smaug), Trailer hitch (Tral), Maternal expression at 31B (Me31B), marks the MZT (CAO *et al.*
700 2020). We thus decided to probe, using antibodies generated against these proteins (Fig. 7) if
701 the degradation of any of these proteins is affected due to maternal loss of Casp/*casp* during
702 the initial hours of embryonic development (0-1, 1-2 & 2-3 hours). TER94 protein is unchanged
703 (Fig. D1, D2) as is the α-tubulin loading control (Fig. 7E1, E2). Furthermore, pattern of
704 degradation of Me31B and TRAL proteins in the *casp*^{lof} embryos is relatively unaffected, when
705 compared to the *w*^{1118} control samples.
706
707
708
709
710
711
712
713
714
715
716
717
718
719
720
721
722
723
724

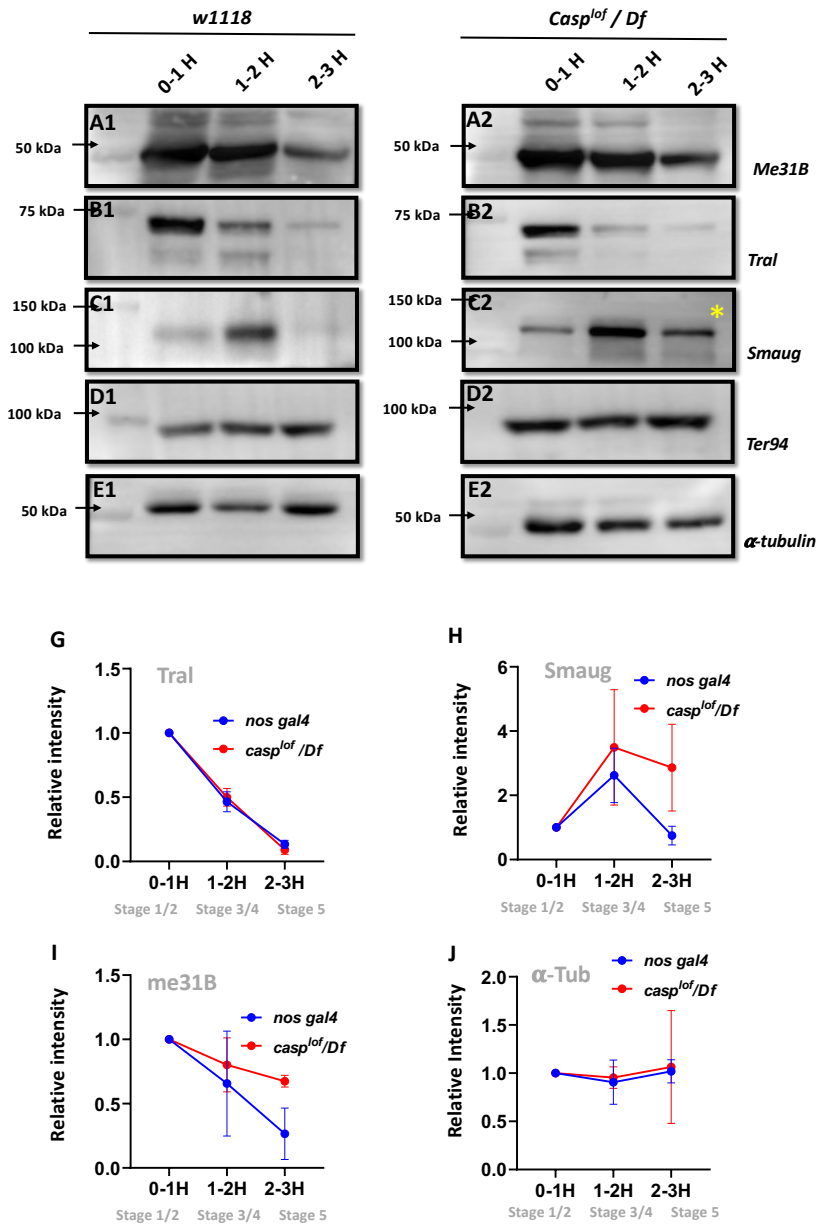

Fig. 7. Reduction in Casp activity specifically affects Smaug degradation during the MZT. At the MZT, a few maternal proteins are actively degraded (CAO *et al.* 2020). Embryos from mothers with genotype w^{1118} **(A1-E1)** and $casp^{lof}/Df$ **(A2-E2)** were collected using three time intervals (0-1, 1-2, 2-3 Hrs), and embryonic lysates were separated on SDS-PAGE gels. The Western blots were probed with antibodies against ME31B (A1-A2), Tral (B1-B2) and Smaug (C1-C2) to assess the extent of protein degradation, as part of the MZT. α-tubulin (E1-E2) was used as a loading control, while TER94 (D1-D2) was used as a negative control as it is a maternal protein that does not undergo degradation at MZT. (**G-J**) Quantitation of the intensity of change of protein band (normalized to 1), for Tral (G), Smaug (H), ME31B (I) and tubulin (J). Each data point is an average of over 5 western blots.

By contrast, Smaug (Fig, C1-C2) is an interesting exception. In control, 0–1hr old embryos, low levels of Smaug protein were observed, which increased in the 1-2hr old embryo extract but decreased the 2-3 hr time-window (Fig. 7C), data that agrees with previously published work (CAO *et al.* 2020). However, in the *casp^{lof}/Df* embryos levels of Smaug protein are modestly elevated from the start (0-1 and 1-2 hr old extract samples respectively; Fig. 7C2). Critically, unlike control embryos, Smaug protein persists in 2-3hr old *casp^{lof}/Df* embryonic extracts (Fig 7C2, *). Altogether, these data argue that Smaug degradation is specifically adversely influenced in the *casp^{lof}/Df* embryos at the end of the MZT.

Germ cell specifc Smaug levels are influenced by casp activity.

Since Smaug levels appear to be elevated in embryonic lysates in the MZT, we decided to test if the Smaug levels are elevated specifically in *casp^{lof}/Df* pole cells. To this end, pre-syncytial as well as early syncytial blastoderm embryos of both the genotypes (control and *casp^{lof}/Df*) were stained with anti-Smaug and anti-Vasa antibodies. Aligned with the Western blot data presented earlier, levels of Smaug protein are significantly elevated in pre-syncytial embryos (Fig. 8, compare panel B3 with A3). Also, in *casp^{lof}/Df* embryos, Smaug protein seems to accumulate in discernible large puncta which are barely visible at this stage in control embryos (Fig. 8, B3 vs A3). At the syncytial blastoderm stage (Stage 4), however, the Smaug positive puncta appear larger and more numerous in the few surviving PGCs from the *casp^{lof}/Df* embryos (Fig. 8, D3) when compared to controls (C3).

Taken together, our data suggest that Smaug protein levels are appreciably elevated in pole cells from *casp^{lof}/Df* embryos. The specific increase in Smaug levels may, in part, be due to inappropriate accumulation and/or stabilization of Smaug. Smaug protein is necessary for translational control of the posterior determinant *nanos*. Early reports indicated that unlocalized *nos* RNA is translationally repressed by Smaug which binds to Smaug Response Elements (SREs) within 3'UTR of *nos* RNA. In addition to *nos*, it also regulates *hsp83* translation. Smaug participates in multiple, overlapping mechanisms including interaction with the components of the translation machinery as well as deadenylation to regulate translation/localization of the target RNAs (DAHANUKAR *et al.* 1999; ZAESSINGER *et al.* 2006).

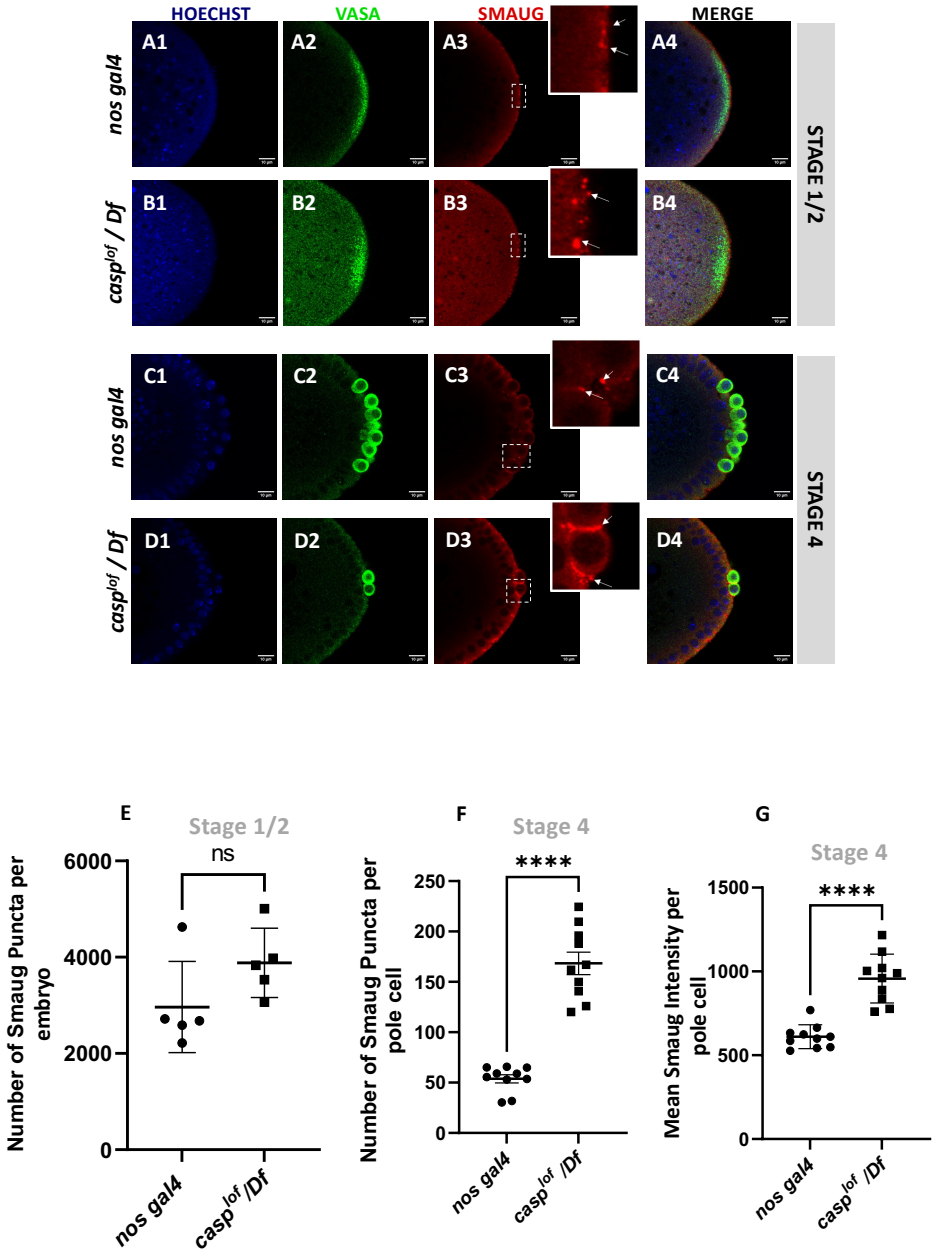

Fig. 8. Decrease in Casp correlates with an increase in Smaug levels in the pole buds and PGCs. Confocal microscopy images of the posterior termini of stage 1-2, and 4 embryos derived from *nos gal4* and *casp^{lof}/Df* females. Embryos were immunostained with Vasa (green) and Smaug (red) antibodies. Hoechst marks the nuclei (A-D). Smaug expression was quantified across the two genotypes and plotted as bar graphs (E-G). N=5 embryos (Stage 2) and 10 embryos (Stage 4).

Intriguingly, recent data from Lipshitz lab has, in fact, shown that Smaug protein accumulates in germ granules (SIDDIQUI *et al.* 2023). Moreover, in addition to its canonical role in regulating *nos* translation, it can also repress *oskar* at the translational level (see Discussion).

868 As the embryonic PGC count depends upon Oskar levels, *Smaug* mutant embryos show an
869 increase in the total number of PGCs. These data fit nicely with our observations and are
870 entirely consistent with a model incorporating the downregulation of Smaug mediated by Casp.
871
872 ***Functional analysis of different protein domains within Casp.***
873 To decipher the specific functions of the individual protein domains of Casp during pole
874 cell formation and division we followed an experimental strategy involving rescue of the loss of
875 function phenotype. We compared the extent of rescue observed in the presence of individual
876 deletion constructs to the full length wild-type control. To this end, fly lines expressing domain
877 deletions of Casp under the *pUASp* promoter were generated (Fig. 9A). The *pUASp-casp*$^{\Delta UBA}$,
878 *pUASp-casp*$^{\Delta UBX}$ and *pUASp-casp*$^{\Delta UAS}$ construct represent deletions of the UBA, UBX, and UAS
879 domains, respectively. Additionally, we also generated fly lines that express the *pUASp-*
880 *casp*$^{\Delta UAS\Delta UBX}$ which deletes both the N and C-terminal domains simultaneously. A full-length
881 coding sequence of Casp was also cloned, and this *pUASp-casp*^{WT} line was used as a positive
882 control carrying the 'rescue' construct. A western blot confirmed the expression of these
883 constructs in adult animals with different domain deletions (Δ), *UAS-casp*$^{\Delta}$ driven by *nos-GAL4*
884 driver (Fig. 9B). To assess the domain-specific functions of Casp in isolation without the
885 confounding effects of endogenous Casp, the fly lines were balanced with a *casp*^{lof} allele on the
886 second chromosome. These balanced lines were crossed to a fly line with the maternal driver
887 *nos-GAL4* on the third chromosome and an allele with a deficiency for *casp (Df)*. Embryos laid
888 by mothers of the genotype *casp*^{lof}*/Df; nos-GAL4/pUASp-casp*$^{\Delta}$ were used to determine
889 maternal effects of the domain deletions (Fig. 9C).

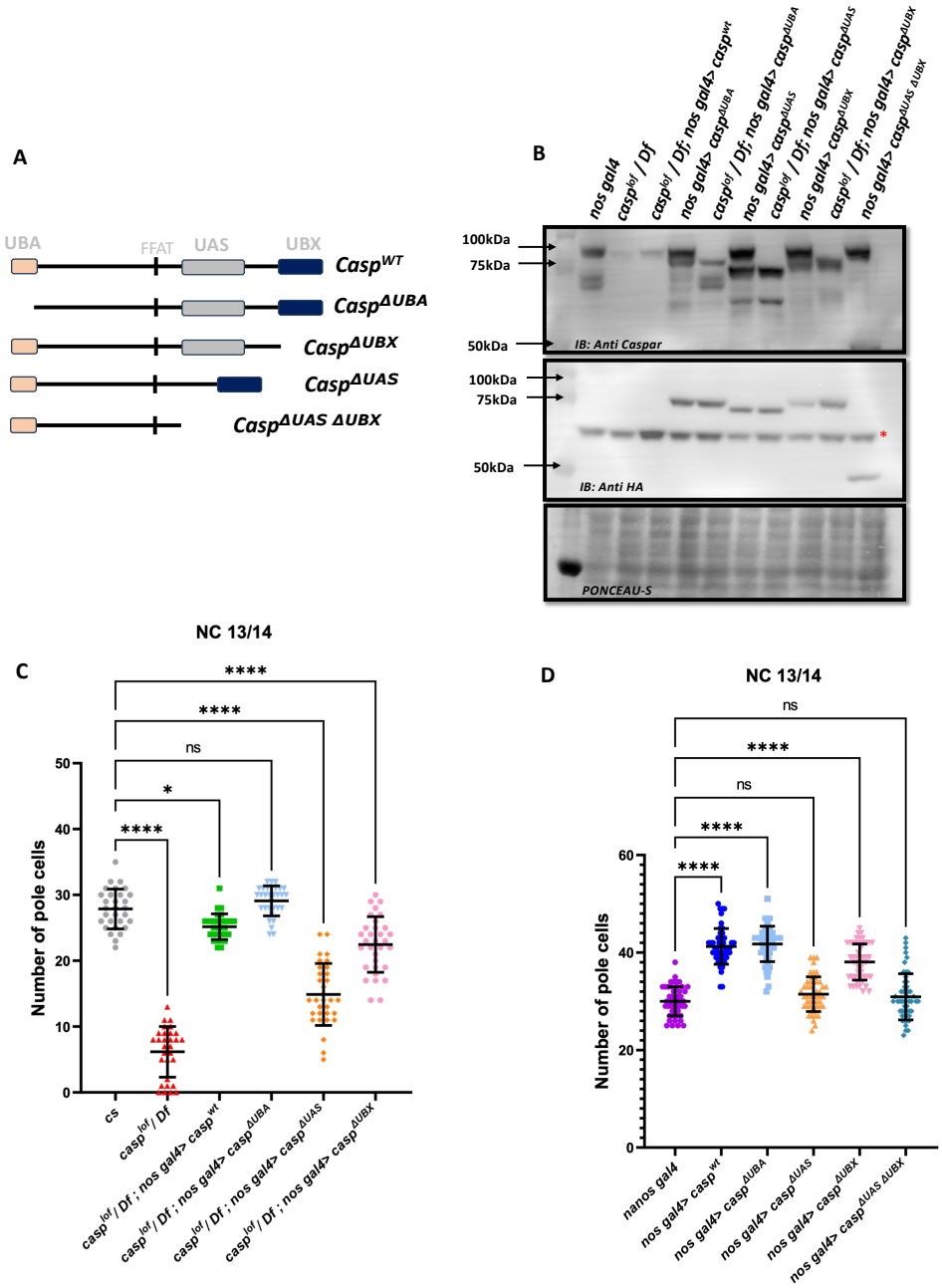

Fig. 9. Structure-function analysis of Casp protein domains in regulating pole cell number. (A) Schematic representation of different domain deletion variants of Casp. As shown in the schematic, the WT Casp protein consists of different functional domains including UBA, UAS, UBX and the FFAT-like motif. **(B)** Western blot of the truncated Casp proteins, deficient in the domains indicated, probed with rabbit anti-casp (1:10,000) and rabbit anti-HA (1:2000) antibody. *nos gal4* served as a control. Ponceau staining was used as a loading control. Asterisk (*) denotes non-specific antibody binding. **(C)** The total number of germ cells from nc 13/14 embryos derived from mothers expressing different *casp* domain deletion constructs in the *casp^{lof}/Df* background were marked with Vasa antibodies, quantified and plotted as a bar graph. n = 30, Ordinary one-way ANOVA, (****) P <0.0001, (*) $P<0.05$. **(D)** The total number of germ cells from nc 13/14, derived from mothers expressing casp domain deletion, in an otherwise *wild-type* background, were stained with anti-Vasa antibodies. Vasa positive cells (i.e. PGCs) were quantified and plotted as a bar graph. n = 30, Ordinary one-way ANOVA, (****) P <0.0001.

946

947 Embryos were collected from females of different genotypes and stained using anti-Vasa
948 antibodies. As can be seen by the comparison shown in the bar graph (Fig. 9C), in terms of the
949 rescue of PGC numbers, deletion of the UBA domain does not affect the rescuing activity of the
950 Casp protein, the UBX domain deletion can rescue, but is weaker than the UBA domain
951 deletion, whereas deletion of the UAS domain is the least effective with regards to the rescue.
952 To extend these observations, we overexpressed individual Casp deletion mutants in an
953 otherwise wild-type background and counted the total number of PGCs. Neither the maternal
954 overexpression of *pUASp-casp*^{wt} nor any of the *pUASp-casp*$^{\Delta}$ increased lethality in terms of
955 decrease in hatching of embryos, in all cases the hatching was in the range 90-95%. Again, as
956 seen before, overexpression of *casp*^{wt} under these conditions led to a significant increase in the
957 total number of PGCs in blastoderm embryos, with average PGC's at 40. The ability to enhance
958 the PGC division is retained in the absence of the UBA domain as, in this particular background,
959 the mean count of the total number of germ cells was similar to embryos that expressed full-
960 length protein. By contrast, deletion of the UAS domain is unable to support the (increased)
961 germ cell division, and the total PGC count dropped to the same level as *nos Gal4* embryos.
962 Interestingly, deletion of UBX domain, yet again, displayed intermediate activity, with the *ΔUBX-*
963 *ΔUBA* domain deletion also being unable to drive the increase in PGCs.
964 Proteomic analysis of the embryonic extracts suggested that in addition to
965 TER94 protein, Casp is also associated with VAP (Fig. S4A; (TENDULKAR *et al.* 2022)). We thus
966 sought to test if physical interaction between Casp and VAP is relevant for pole cell formation.
967 To assess this possibility, we used a deletion variant of Casp, Casp$^{\Delta FFAT}$, which cannot interact
968 with VAPB (TENDULKAR *et al.* 2022). Expression of *casp*$^{\Delta FFAT}$ under the control of maternal
969 driver, in a *casp*^{lof}/Df mother showed hatching (~60%) frequencies at par with wild type (Fig.
970 S4B), with expression levels equal to other *casp* constructs (Fig. S4C). Importantly, *nos-Gal4-*
971 dependent maternal overexpression *of UAS-casp*$^{\Delta FFAT}$ led to an increase in the total number of
972 PGCs in syncytial blastoderm embryos, comparable to full-length *UAS-casp*^{wt} (average PGC
973 ~23). Lastly, expression of *casp*$^{\Delta FFAT}$ could rescue the PGC loss upon maternal loss of *casp*
974 (compare Fig. S4 F1-3 to Fig. 9C). These data suggested that interaction between Casp and
975 VAP is either not essential or partially redundant for Casp function in the context of determining
976 PGC. Altogether, the functional analysis of different protein domains within Casp underscores
977 the importance of UAS and UBX domains, especially in embryonic contexts, including PGC
978 development.
979

Materials & Methods

Fly husbandry and stocks*:* Flies were raised on standard cornmeal agar at 25 °C unless stated otherwise. *Casp*^{lof} (11373), *Casp Df* (23691), *nos Gal4* (4937), *Mat* α*4-tubulinGal4:VP16* (7063) and *TER94 RNAi* (32869) lines were procured from the Bloomington *Drosophila* Stock Centre, with numbers in brackets indicated Stock numbers.

Cloning of *casp* deletion constructs and generation of transgenics*:* UASp-casp$^{\Delta}$ constructs (*pUASp casp*$^{\Delta UBA}$*, pUASp casp*$^{\Delta UAS}$*, pUASp casp*$^{\Delta UBX}$*, pUASp casp*$^{\Delta UAS\Delta UBX}$) were generated, starting from a *pUASp-attB-Casp* construct (TENDULKAR *et al.* 2022), with the design including an N-terminal HA tag. The constructs were injected into a *w*^{1118}*; Attp2* embryo in the NCBS-CAMP transgenic injection facility (https://www.ncbs.res.in/research-facilities/drosophila-services), and stable lines were generated by balancing against a *w*^{1118}*; TM3Sb/TM6Tb* animal.

For cloning and amplification, a functional N-terminal HA tag was introduced with the 5'-forward primers and a 3'-homology arm was introduced using the 3'-reverse primers. The exception was the *pUASp Casp*$^{\Delta UAS}$ construct where two fragments, one upstream and one downstream of the UAS domain were amplified separately with 22 nucleotide homologous overhang between them to mediate homologous recombination. The upstream fragment contained the HA sequence while the downstream fragment contained the 3'-homology arm. The sequences of the primers used are as follows. *TGTTCCAGATTACGCTGGCGGC* was used as the 5'-forward primer for the *pUASp casp*^{wt}, *pUASp casp*$^{\Delta UBX}$, *pUASp casp*$^{\Delta UAS\Delta UBX}$ and the upstream fragment of the *pUASp casp*$^{\Delta UAS}$ constructs.
TGTTCCAGATTACGCTGGCGGCCCCCATCCTATCCTGGTGCC was used as the 5'-forward primer for the *pUASp casp*$^{\Delta UBA}$ construct.
CGGATGATGAGATAAGTGGCTCCACGGAAACATGCGAAATGTTTGAGGAGCAG was used as forward primer for amplifying downstream fragment of the *pUASp casp*$^{\Delta UAS}$ construct.
ACCATGGGTTTAGGTATAATGTTATCAAGCTCC was the reverse primer for *pUASp casp*^{wt}, *pUASp casp*$^{\Delta UBA}$, and downstream fragment of *pUASp casp*$^{\Delta UAS}$.
TTAGGTATAATGTTATCAAGCTCCTCATTCGGACGGCTCCTGAGGTAG was the reverse primer for *pUASp casp*$^{\Delta UBX}$.
TTAGGTATAATGTTATCAAGCTCCTCACGTGGAGCCACTTATCTCATCATCCG was used as the reverse primer for *pUASp casp*$^{\Delta UAS\Delta UBX}$. *CGTGGAGCCACTTATCTCATCATCCG* was the reverse primer for upstream fragment of *pUASp casp*$^{\Delta UAS}$. PCR products were further amplified with a common 5'-primer
ATAGGCCACTAGTGGATCTGATGTACCCATACGATGTTCCAGATTACGCTGGCGGC and

1013 their respective reverse primers to introduce the 5'-homology arm. Inserts were recombined into
1014 *pUASp AttB* vector linearised at the BamH1 site, using a variation of the SLiCE cloning method
1015 (ZHANG *et al.* 2012; ZHANG *et al.* 2014). In short, E.coli DH10B expressing the optimised **λ**-
1016 prophage red recombinase system (PPY cells) was cultured in the presence of arabinose to
1017 induce recombinase expression and subsequently used for preparing competent cells. DNA
1018 fragments containing homologous overhangs were co-transformed into the competent bacteria
1019 and resultant colonies were screened through PCR to identify proper recombinants and
1020 subsequently confirmed through sequencing.The pUASp *casp*$^{\Delta FFAT}$ was PCR amplified from
1021 *pRM-HA:casp* $^{\Delta FFAT}$ (TENDULKAR *et al.* 2022), cloned into pUASp-AttB, sequenced for validation
1022 and injected into a *w*^{1118}*; Attp2* animal.
1023 **Embryonic lethality***:* 0-3 hr embryos were collected, transferred to a fresh sugar-agar plate,
1024 and unhatched larvae were scored after 48 hours to determine viability.
1025 **Immunoprecipitation***:* 0–3-hour embryos were lysed in Co-IP Lysis Buffer (20mM Tris pH 8.0,
1026 137mM NaCl, 1% IGEPAL, 2mM EDTA, 1X PIC) using a Dounce homogenizer, and centrifuged
1027 at 21,000 g for 30 minutes. 3 mg of total lysate was incubated with 5 µg of primary antibody (Rb
1028 anti-Casp) and 5 µg of Normal Rabbit IgG overnight at 4 °C. Antigen-antibody complexes were
1029 captured using 50 µL of BioRad SureBeads Protein A (1614013) at 4 °C for 4 hours. Beads
1030 were washed six times with Co-IP Lysis Buffer and protein complexes eluted by boiling in 1X
1031 Laemmli Sample Buffer. Eluted proteins were resolved on a 10% polyacrylamide gel followed by
1032 western blotting or in-gel trypsin digestion, described in the following sections.
1033 **Western blot analysis***:* Embryos collected at varied time points (0-3, 0-1, 1-2, 2-3 hours) were
1034 lysed in RIPA buffer (50 mM Tris-Cl, 150 mM NaCl, 0.1% SDS, 0.01% Sodium azide, 0.5%
1035 sodium deoxycholate, 1 mM EDTA, 1% Triton X-100, 1X PIC) with a pellet pestle (Kontes).
1036 Lysates were cleared by centrifugation at 21,000 g at 4 °C for 30 minutes. Protein concentration
1037 was estimated using a BCA assay (Pierce) and 30-40 µg of total protein was loaded onto the gel
1038 after boiling in 1X Laemmli Sample Buffer. Proteins separated by 10% SDS-PAGE were
1039 transferred onto a PVDF membrane (Immobilon-E, Merck) and blocked in 5% milk in Tris-Buffer
1040 Saline (TBS) with 0.1% Tween 20 (TBS-T) for an hour. Blots were then incubated overnight with
1041 primary antibody diluted in 5% milk in TBS-T, at 4 °C. Following three washes with TBS-T, blots
1042 were incubated with secondary antibodies diluted in 5% milk in TBS-T, for 1 hour at room
1043 temperature. Blots were washed thrice with TBS-T and visualized on a LAS4000 Fuji imaging
1044 system after incubating with Immobilon Western Chemiluminescent HRP substrate (Merck). The
1045 following antibodies were used: Rabbit anti-VAP, 1:10000 (TENDULKAR *et al.* 2022), Mouse anti-
1046 α-Tubulin, 1:10000 (T6074, Sigma), Mouse anti-Ubiquitin, 1:1000 (P4D1, Santa Cruz

1047 Biotechnology), Mouse anti-HA, 1:5000 (H3663 HA-7, Sigma-Aldrich), Rabbit anti-Casp,
1048 1:10000 (TENDULKAR *et al.* 2022), 1:2000 (04-902 DW-2, Sigma-Aldrich) Goat anti-rabbit HRP
1049 and Goat anti-mouse HRP secondary antibodies, each at 1:10000 (Jackson ImmunoResearch).
1050 Rabbit anti-me31B, 1:1000, Rabbit anti-Smaug, 1:500, Rat anti-Tral, 1:1000 were a kind gift
1051 from Elmar Whale (CAO *et al.* 2020).
1052 **In-gel Trypsin Digestion and LC-MS/MS Analysis***:* Before in-gel trypsin digestion of the Co-IP
1053 eluate, the antibody was crosslinked to the SureBeads using DMP (Sigma) according to the
1054 NEB crosslinking protocol to avoid elution of the antibody. After crosslinking 10µg Casp
1055 antibody, Co-IP was performed as described above. In-gel trypsin digestion was carried out as
1056 previously described (SHEVCHENKO et al. 2006). Briefly, Coomassie-stained bands on the gel
1057 were excised and cut into 1 mm cubes. Gel pieces were transferred to a clean microcentrifuge
1058 tube and destained with buffer containing 50% acetonitrile in 50 mM Ammonium bicarbonate.
1059 Reduction and alkylation were carried out on the destained gel pieces by incubating with 10mM
1060 dithiothreitol (DTT) followed by incubating with 20mM iodoacetamide. Gel pieces were saturated
1061 with sequencing grade Trypsin (Promega) at a concentration of 10 ng/µL and incubated
1062 overnight at 37 °C. Peptides were extracted by sequential addition of 100 µl of 0.4%
1063 Trifluoroacetic acid (TFA) in 10% ACN, 100 µl of 0.4% TFA in 60% ACN and 100 µl of ACN.
1064 The pooled extract was dried in a vacuum centrifuge and reconstituted with 50 µl of 0.1% TFA.
1065 The peptides in TFA were purified using the StageTip protocol (RAPPSILBER et al. 2007). LC–
1066 MS/MS analysis was performed on the Sciex TripleTOF6600 mass spectrometer interfaced with
1067 an Eksigent nano-LC 425. Tryptic peptides (1 µg) were loaded onto an Eksigent C18 trap (5 µg
1068 capacity) and subsequently eluted with a linear acetonitrile gradient on an Eksigent C18
1069 analytical column (15 cm × 75-µm internal diameter). A typical LC run lasted 2 h post loading
1070 onto the trap at a constant flow rate of 300 nL/min with solvent A consisting of water + 0.1%
1071 formic acid and solvent B consisting of acetonitrile. The gradient schedule for the LC run was
1072 5% (vol/vol) B for 10 min, a linear gradient of B from 0% to 80% (vol/vol) over 80 min, 80%
1073 (vol/vol) B for 15 min and equilibration with 5% (vol/vol) B for 15 min. Data was acquired in an
1074 information-dependent acquisition (IDA) mode over a mass range of 300–2,000 m/z. Each full
1075 MS survey scan was followed by MS/MS of the 15 most intense peptides. Dynamic exclusion
1076 was enabled for all experiments (repeat count 1; exclusion duration 6 s). Peptides were
1077 identified and quantified using the SCIEX ProteinPilot software at a false discovery rate (FDR)
1078 of 1%. A RefSeq *Drosophila* protein database (release 6) was used for peptide identification.
1079 Proteins that were identified in two or more replicates were tabulated.

1080 **Fixation, immunostaining, and imaging of embryos***:* 0-3 hr embryos were collected in a
1081 sieve and dechorionated in 4% sodium hypochlorite for 90 seconds. After thorough washes with
1082 distilled water, embryos were fixed in a 1:1 heptane:4% PFA solution for 20 minutes. The PFA
1083 layer was removed, and embryos in heptane were re-constituted with an equal volume of
1084 methanol. Embryos were devitellinized by vigorous shaking in the 1:1 heptane:methanol
1085 mixture. The heptane layer and the interphase containing non-devitellinized embryos were
1086 carefully removed. Devitellinized embryos in the bottom methanol phase were washed twice
1087 with methanol and stored at -20 °C till they were ready to be imunostained. For phalloidin and
1088 Smaug staining, embryos fixed in heptane: 4% PFA were hand de-vitellinized, after which the
1089 standard immunostaining procedure was followed. For immunostaining, embryos were
1090 rehydrated by washing thrice with 0.3% PBS-TritonX 100 (PBS-T) for 15 minutes each.
1091 Embryos were blocked in 2% BSA in 0.3% PBS-T for 1 hour at room temperature (RT).
1092 Embryos were incubated at 4 °C overnight with primary antibodies diluted in 2% BSA in 0.3%
1093 PBS-T at the appropriate dilutions. Following three 15-minute washes with 0.3% PBS-T,
1094 embryos were incubated in the appropriate secondary antibodies for 1 hour at room
1095 temperature. The following antibodies were used: Rabbit anti-Casp, 1:1000 (TENDULKAR *et al.*
1096 2022); Rat anti-α-vasa; 1:50 (DSHB); Rabbit anti-VCP, 1:200 (#2648, Cell Signaling
1097 Technology); Rabbit anti-Oskar, 1:1000 (generated by Mandy Jeske, Anne Ephrussi lab); Rabbit
1098 anti-Smaug, 1:50; Mouse anti-γ-tubulin, 1:1000 (T6557, Sigma), Rabbit P-Histone H3 (S10)
1099 1:300 (#9701, Cell Signalling); Alexa Fluor 568 Phalloidin, 1:1000 (Invitrogen) The following
1100 secondary antibodies were used, goat anti-mouse Alexa488/ goat anti-rabbit Alexa568/ goat
1101 anti-rat Alexa647/ goat anti-rabbit Alexa647/ goat anti-rabbit Alexa480, 1:1000 (DSHB).
1102 Embryos were washed thrice with 0.3% PBS-T, and DAPI/Hoechst (1:500) was added in the
1103 penultimate wash. Embryos were mounted in 70% glycerol and observed under a Leica sp8
1104 confocal microscope with a 20X objective.
1105 **Live imaging of embryos***:* Embryos at the appropriate stage were washed and dechorionated
1106 as described previously. A 2-well Nunc™ Lab-Tek™ II Chamber Slide™ System (ThermoFisher
1107 Scientific) was affixed with a 3M Scotch double-sided tape, and dechorionated embryos with
1108 intact vitelline membranes were mounted on the tape under a dissecting microscope.
1109 Halocarbon oil 200 was used to cover the embryos to prevent dehydration during imaging.
1110 Time-lapse imaging of embryos was performed on an inverted LSM confocal system (Zeiss
1111 multiphoton 710) at 20X for ~8 hours. Embryo images were acquired at 5 min intervals.
1112

Quantification of western blots: Western blots were quantified using ImageJ. Each protein was normalized to the tubulin loading control, and the highest signal for each was set to 1 and all other tubulin band intensities were normalized against it. For MZT experiments, western blots were used to determine protein degradation dynamics. 3-5 biological replicates, representing 3-5 independent embryo collection were assayed. Band intensities were quantified using ImageJ and normalized to α-tubulin as loading control. For each replicate intensities were normalized to the first time point (0-1 hour). Significance thresholds are presented in the figures and figure captions.

Quantification of the Smaug Immunostaining: All quantification of Smaug stained images were done on ImageJ. ROIs were made for a single pole cell through the z-stacks, thereby only analysing one pole cell at a time. For each embryo five such pole cells were measured. To quantify intensity, mean intensity was measured for each ROI per stack and added to get the final intensity. Each data point on the graph represents an average of all five cell intensities per embryo. For Smaug punctae measurement, a combined ROI for each cell was taken and duplicated. Each of the stack was then analysed using 3D objects counter, where thresholding for all images was kept within the range of 80-90 with a minimum size filter kept at zero. The number of objects counted was taken as the total number of Smaug punctae per cell. Five such pole cells were analysed per embryo and the average was plotted as a single data point on the graph. For quantification of poleplasm volume in the embryos, embryos were stained with Oskar. An ROI (kept same for all images) encompassing the posterior part of the embryo was drawn. Gaussian blur 3D (X sigma = 2, Y sigma = 2 and Z sigma = 2) was applied to each image. The volume of pole plasm was analysed by using 3D objects counter after appropriate thresholding.

1138 **Discussion**

1139 Proper development of biological systems in an organismal context involves complex
1140 interactions between various individual pathways. The qualitative nature of the interaction(s)
1141 between pathway components ultimately determines how different pathways intersect in a
1142 context-specific manner. Curiously however, there are only a defined number of signaling
1143 pathways/circuits that have been elucidated thus far. Consistently, the entire molecular
1144 cassettes that constitute a given pathway or a select number of pathway components, are
1145 reiteratively used in a variety of biological contexts even within a lifecycle of the same organism.
1146 Moreover, while such repurposing is relatively frequent, the corresponding biological outcomes
1147 are diverse in nature and insightful in ways more than one. Our data detailing the functional
1148 involvement of Casp and TER94 in the PGCs is a case in point. Casp function was initially
1149 characterized in the context of *Drosophila* immune response (KIM *et al.* 2006). However, the
1150 original study did not investigate the developmental roles of Casp and its interactors. Here, we
1151 report novel activities of *Drosophila melanogaster* immune components Casp and TER94 during
1152 early embryonic development with a specific focus on germline.

1153 Early embryonic patterning is a dynamic process in metazoans which is primarily
1154 regulated by the deposition of maternal gene products including RNAs and proteins. Such
1155 maternal determinants are localized in a spatially restricted manner (SCHIER 2007). On many
1156 instances, the unique pattern of localization of specific factors underlies their activities during
1157 embryo patterning. To execute their functions properly, patterning determinants heavily rely
1158 upon the members of the housekeeping machinery that carefully calibrate the synthesis,
1159 stability, transport, and degradation of diverse regulatory components. Here, we have explored
1160 novel embryonic functions for the FAF1 ortholog, Casp in *Drosophila*. Initially, we uncovered
1161 that maternal loss of *casp* activity results in partially penetrant embryonic lethality. The *casp*
1162 allele was determined to be a strong loss of function, but not a null. The partial penetrance could
1163 also be due to redundancy. Consistent with either possibility, quantitation of the individual
1164 phenotypes yielded significant but variable penetrance.

1165 In keeping with a semi-vital function, our data demonstrated its involvement during
1166 cellular movements that lead to gastrulation, a likely cause underlying the lethality. Surprisingly,
1167 Casp protein is enriched in the PGCs, which are specified at the posterior pole under the control
1168 of the master germ cell determinant, Oskar. PGC formation and specification in a young
1169 *Drosophila* embryo depends on the posteriorly anchored specialized cytoplasm (or pole plasm)
1170 enriched in RNA and protein components essential to determine germ cell identity and behavior.
1171 Two important traits distinguishing early pole cells from the surrounding somatic nuclei include

1172 precocious budding and limited mitotic self-renewal. Consistent with its functional involvement in
1173 both these processes, maternal loss of either Casp or its protein partner TER94 resulted in a
1174 reduced number of buds and subsequent loss of PGCs. While qualitatively similar, the severity
1175 of phenotypic consequence due to loss of Casp and TER94 regarding PGC loss, is not identical.
1176 Interestingly, however, both proteins appear to influence centrosome behavior and dynamics
1177 that are of paramount significance in forming pole cells in *Drosophila* embryos.
1178 Thus far, Germ cell-less (Gcl) is the only protein shown to control PGC formation in a
1179 similar manner (JONGENS *et al.* 1992). Importantly Gcl activity depends on its ability to influence
1180 proper separation of centrosomes and elaboration of astral microtubules in dividing pole buds
1181 (LERIT *et al.* 2017). Aberrant centrosome behavior in *gcl* mutant embryos adversely affects PGC
1182 budding and equitable distribution of germ plasm among daughter cells. Intriguingly, these
1183 phenotypic traits can be recapitulated by simply engineering defective centrosome separation
1184 (LERIT *et al.* 2017). It is thus noteworthy that maternal loss of Casp and TER94 leads to similar
1185 defects and future experiments will reveal mechanistic details underlying roles of these two
1186 proteins in regulating centrosome dynamics in PGCs and their possible interaction with Gcl and
1187 its protein partners. Of note, a germplasm interactome (THOMSON *et al.* 2008) included TER94
1188 along with other important germ plasm proteins including Vasa, Tudor, and others.
1189 TER94, an ER protein, is a major Casp interactor. Our data also indicate that in addition
1190 to PGC formation, TER94 and Casp regulate early nuclear division cycles in syncytial
1191 blastoderm embryos and subsequent cell divisions in the somatic compartment cell cycle
1192 processes in the gastrulating embryos. (Casp and TER94 are distinct compared to Gcl in this
1193 regard which has a strictly germ cell specific function). Taken together, these observations
1194 suggest that Casp and TER94 contribute to critical early developmental functions leading to
1195 mid-blastula transition which precedes gastrulation and germband extension. In the mammalian
1196 context, the FAF1-VCP interaction is mediated by the UBX domain. Thus, it is unsurprising that
1197 deletion of the protein domain crucial for association between Casp and TER94 resulted in a
1198 somewhat diminished function as compared to a full-length version. Curiously however, deleting
1199 UAS fragment, a protein domain of unknown function, implicated in self-association, resulted in
1200 substantially compromised activity as compared to native protein. Future experiments will focus
1201 on the specific molecular interactions this (and other) individual domain(s) are involved in. It will
1202 be also important to determine how protein degradation especially engineered via ubiquitin
1203 modification contributes to Casp stability and function.
1204 Intriguingly our data also argue that regulation mediated by *casp* is likely critical for
1205 maintenance of PGC fate via maintenance of Oskar levels. Importantly, several independent

1206 observations suggest that this influence is likely zygotic. First, barely detectable amount of
1207 Casp protein is deposited in the egg and bulk of the Casp protein is generated by translation
1208 post-fertilization. Second, Casp protein controls overall levels of Smaug at the post-
1209 transcriptional level including in the early embryonic PGCs. It was recently reported that Smaug
1210 protein accumulates in the germ granules where it controls Oskar (and Bruno) translation
1211 negatively by binding to Smaug response elements present in the untranslated regions within
1212 the respective RNAs (SIDDIQUI *et al.* 2023). Consistently loss of function mutations in *Smaug*
1213 result in a modestly elevated PGC count in stage 4-5 embryos whereas a reciprocal phenotype
1214 is observed in *casp*^{lof} embryos. Taken together with the increase in Smaug levels in *casp*^{lof}
1215 embryos, it would be reasonable to propose that PGC-specific phenotypes observed upon loss
1216 of *casp* are, in part, mediated by excess accumulation of Smaug. Moreover, these authors also
1217 suggest that Smaug dependent regulation of *oskar* RNA likely has a significant zygotic i.e.
1218 embryonic component which aligns well with our data. Future experiments will be necessary to
1219 elucidate the mechanism underlying regulation of Smaug levels by Casp. It will also be
1220 interesting to examine if Smaug and Casp regulate centrosome behavior reciprocally to control
1221 the final PGC count.
1222 Degradation of maternally deposited RNAs and proteins constitutes an important
1223 transition during embryonic development. Zygotic Genome Activation (ZGA) and turning over of
1224 maternal determinants (Both RNAs and proteins) happen almost simultaneously. Together
1225 these two events constitute MZT which is delayed in the germ cell compartment as opposed to
1226 soma. Nonetheless, recent data have suggested that the two events possibly occur in a
1227 coordinated manner possibly via shared components (COLONNETTA *et al.* 2023). Many of the
1228 embryonic phenotypes that *casp*^{lof} embryos display (aberrant nuclear migration, cellularization
1229 defects, defective gastrulation etc.), are shared by mutations in gene products either directly or
1230 indirectly involved in one of these processes. It will be important to elucidate new interactors of
1231 Casp as its function likely impacts protein degradation and/or stability of the target proteins.
1232 Recent reports have indicated potential involvement of ZGA regulators such as Zelda and
1233 CLAMP in germline/soma distinction. Critically this function of the components of ZGA depends
1234 on proper anchoring, release and transmission of posteriorly anchored pole plasm that involves
1235 centrosome function. Maternally compromising ZGA components resulted in inappropriate
1236 release and transmission of pole plasm RNAs, a phenotype that is partially recapitulated in
1237 *casp*^{lof} and *TER94i* embryos.
1238 While our data have clearly established the involvement of Casp and TER94 during PGC
1239 formation and specification, further studies will be necessary to elucidate their precise molecular

function(s) underlying this activity. Several observations are noteworthy in this regard and will guide the course of future investigation. The first set of results points to the possible participation of both Casp and TER94 during ubiquitin-dependent protein degradation.

A regulatory network incorporating Bru1, Cup, Oskar and Smaug are key to PGC specification. The Skp Cullin and F-box (SCF) containing complex marks proteins such as Smaug for degradation by functioning as an E3 ubiquitin ligase ((CAO *et al.* 2020; CAO *et al.* 2022); Fig. 10A). The ubiquitinated Smaug is then degraded by the proteasome. In the *mammalian* context, the Casp/TER94 orthologs FAF1/VCP (in *green* font; Fig. 10A) have been found to interact with the SCF complex. Our data supports a similar scenario in *Drosophila*.

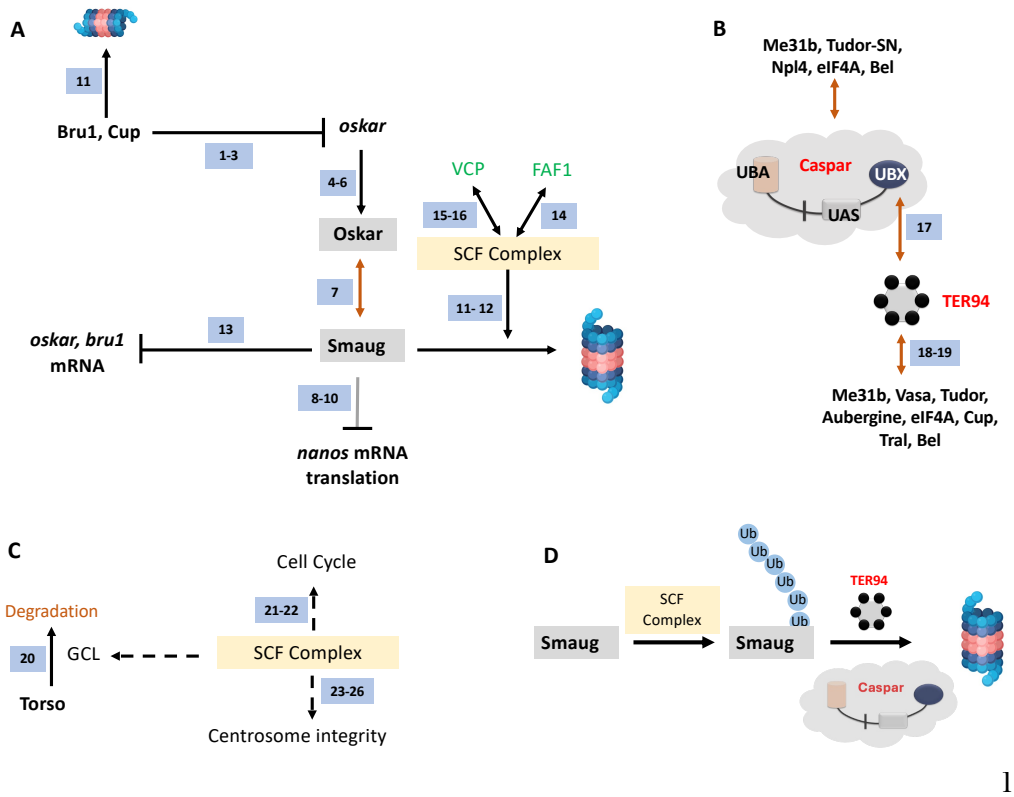

Figure 10. A model for Casp function in PGCs.
(**A**) Smaug is marked for degradation by the SCF complex. Specific pole plasm components including Cup, Oskar and Smaug are actively degraded. *oskar* is regulated by Bru1 and Cup (*ref 1-3*; (NAKAMURA *et al.* 2004; KIM *et al.* 2015; BAYER *et al.* 2023)). Oskar (*ref 4-6*; (MAHOWALD 2001; HUYNH AND ST JOHNSTON 2004; LEHMANN 2016)) is the master determinant of PGC fate, and hence the stability of the Oskar:Smaug complex (*ref 7*;(KUBIKOVA et al. 2023)) is a key to PGC determination and proper specification. Oskar also regulates posterior cell fate by regulating *nos* translation which is modulated by Smaug (*ref 8-10;* (DAHANUKAR et al. 1999; ZAESSINGER et al. 2006; JESKE et al. 2011)). The SCF complex is a multi-protein E3 ubiquitin ligase complex, and Smaug is one of its prominent targets (*ref 11-12;* (CAO et al. 2020; CAO et al. 2022)). Smaug appears to repress the translation of *oskar* and *Bruno 1* mRNA (*ref 13*; (SIDDIQUI *et al.* 2023)). In mammals (marked with green font), FAF1 modulates the SCF complex (*ref 14*; (MORAIS-DE-SA *et al.* 2013)) with VCP/p97 assisting in the degradation of ubiquitinated Smaug (*ref 15-16;* (LI et al. 2014; REIM et al. 2014)), suggesting potential conservation of the activities in the fly orthologs, Casp and TER94.

(**B**) Casp/TER94 interact with an overlapping set of proteins. TER94 has earlier been demonstrated to be associated with Oskar (RUDEN *et al.* 2000). Our data points to an association between *Drosophila* Casp and TER94 (this study and *ref 17;* (TENDULKAR et al. 2022)) that participates in protein degradation. In a proteomic analysis of germ cell components, TER94 was identified (this study and *ref 18*; (THOMSON *et al.* 2008)), along with other bona-fide germ cell constituents including Cup, Tral, Bel, eIF4A, Tud and Vasa (*ref 18* and *19* (THOMSON *et al.* 2008; DEHAAN *et al.* 2017)). Both, Casp and TER94 are thus enriched in the pole cells and interact with proteins that specify PGC fate.
(**C**). The SCF Complex, Gcl and Centrosome integrity. The SCF complex is localized to the centrosome. Gcl interacts with Cullin 3 to degrade Torso receptor to promote PGC fate (*ref 20*; (PAE *et al.* 2017)). The SCF complex regulates the cell cycle (*ref 21-22*; (MARGOTTIN-GOGUET *et al.* 2003; ROGERS *et al.* 2009)) and is a known regulator of centrosomal integrity (*ref 23-26*;(WOJCIK *et al.* 2000; MURPHY 2003; PHUONG THAO *et al.* 2006; CUNHA-FERREIRA *et al.* 2009)), thereby influencing PGC specification (LERIT *et al.* 2017).
(**D**) Casp and TER94 assist in the degradation of Smaug. The SCF complex works as a ubiquitin E3 ligase to mark Smaug for Degradation and PolyUb-Smaug is degraded by the action of Casp and TER94 during the late-MZT.

It would be reasonable to propose that Casp recruits TER94 via Casp's UBX domain (Fig. 10B). Independent proteomic studies ((THOMSON *et al.* 2008; DEHAAN *et al.* 2017; TENDULKAR *et al.* 2022); Fig 10 B) suggest multiple overlaps between Casp/TER94 and germ-cell specific protein complexes (Fig. 10B), again suggesting functional relationships between Casp/TER94 and germ cell determinants. In addition, the SCF complex contributes to cell cycle progression and integrity of centrosomes ((WOJCIK *et al.* 2000; MURPHY 2003; PHUONG THAO *et al.* 2006); Fig 10C). Total PGC count in early embryos depends on centrosome function and efficient mitotic divisions. So SCF complex based degradation may have multiple targets that participate during germ cell formation and specification (Fig. 10C).

Casp likely functions as an adapter protein that works in conjunction with the SCF complex ((CAO *et al.* 2020; CAO *et al.* 2022); Fig. 10D) and TER94 (Fig. 10D). The binary complex between TER94 and Casp subsequently targets ubiquitinated proteins such as Smaug which are present in a complexed form with other proteins. Homeostatic maintenance of Smaug levels via Casp-mediated proteolytic degradation could explain many of our observations. Consistently, increased Smaug levels, due to diminished Casp function leads to loss of PGCs whereas, *smaug* mutant embryos show the opposite phenotype (SIDDIQUI *et al.* 2023). Intriguingly, even though Smaug and Oskar are members of a complex, the reduction in Casp activity results in the stabilization of Smaug. By contrast, Oskar levels are diminished resulting in loss of PGCs. The mechanism underlying the substrate-dependent divergent activities is not known at this point.

The similarity between the phenotypic consequences due to loss of ZGA components and Casp/TER94 also needs a special mention. The only study implicating TER94 during early embryogenesis (ZENG *et al.* 2014) suggested that TER94 can potentiate BMP signaling. Interestingly, *decapentaplegic* (*dpp*), a BMP ligand which is one of the important targets of ZGA

regulators including *Zelda*, can also influence the specification of embryonic PGCs (COLONNETTA *et al.* 2023). PGCs need BMP signals (Dpp) to maintain their identity. Furthermore, the exposure to BMP signals needs careful calibration as excess BMP signaling in the surrounding soma leads to PGC loss. Importantly, components of protein degradation machinery including those involved in ubiquitination (Smurf, a Ubiquitin ligase) and sumoylation (Ubc9) appear to be involved in fine-tuning the signaling (DESHPANDE *et al.* 2014). Thus, it will be of interest to determine if the aberrant germ cell specification observed due to loss of *casp* and the components of BMP signaling pathway is mechanistically connected. This seems especially relevant in the light of their respective dependence on the components of the protein degradation machinery. It will be of considerable interest to investigate whether and how, zygotic activity of Smaug, one of important canonical MBT regulators, fits into this picture. In sum, while the specific details await detailed examination, it is apparent that possible recapitulation of maternal regulation in the zygotic context may be a recurrent theme rather than an isolated anomaly.

Competing interests

The authors declare no competing or financial interests.

Funding

Science & Engineering Research Board (SERB) grant CRG/2018/001218. GD's visits to IISER Pune (2023-2025) are supported by the Ministry of Education (MoE) Scheme for the promotion of Academic & Research Collaboration (SPARC), Grant ID SPARC-1587, managed by IIT Kharagpur, which facilitates collaboration between IISER Pune and Princeton University. The IISER *Drosophila* media and Stock centre are supported by the National Facility for Gene Function in Health and Disease (NFGFHD) at IISER Pune, which in turn is supported by an infrastructure grant from the DBT, Govt. of India (BT/INF/22/SP17358/2016). JS, NW and AR are undergraduates supported by INSPIRE/KVPY fellowships. SD and SH are graduate students supported by fellowships from the Council of Scientific & Industrial Research (CSIR), Govt. of India.

Contributions

SH and SD performed most of the experiments, with contributions from NW, JS, and AR. GR and GD conceptualized the project with input from SH and SD. SH, SD, GR, and GD analyzed

and interpreted the data. GD, GR, SH, and SH wrote the manuscript. GR and GD supervised the project and acquired funding.

Acknowledgements

We thank Bloomington *Drosophila* Stock Center (BDSC), Indiana, supported by NIH grant P40OD018537, for fly stocks; Elmar Whale and Christiane Rammelt for the kind gift of anti-Tral, anti-Me31B and anti-Smaug antibodies; Snehal Patil and Yashwant Pawar for fly media and stock maintenance; IISER Microscopy facility, Dr Santosh Podder and Vijay Vittal for training and maintenance.

1374 **References**

1375 Adams, M. D., S. E. Celniker, R. A. Holt, C. A. Evans, J. D. Gocayne *et al.*, 2000 The genome
1376 sequence of Drosophila melanogaster. Science 287**:** 2185-2195.
1377 Arkov, A. L., J. Y. Wang, A. Ramos and R. Lehmann, 2006 The role of Tudor domains in germline
1378 development and polar granule architecture. Development 133**:** 4053-4062.
1379 Azuma, Y., T. Tokuda, M. Shimamura, A. Kyotani, H. Sasayama *et al.*, 2014 Identification of
1380 ter94, Drosophila VCP, as a strong modulator of motor neuron degeneration induced by
1381 knockdown of Caz, Drosophila FUS. Hum Mol Genet 23**:** 3467-3480.
1382 Bayer, L. V., S. Milano, S. K. Formel, H. Kaur, R. Ravichandran *et al.*, 2023 Cup is essential for
1383 oskar mRNA translational repression during early Drosophila oogenesis. RNA Biol 20**:**
1384 573-587.
1385 Belvin, M. P., and K. V. Anderson, 1996 A conserved signaling pathway: the Drosophila toll-
1386 dorsal pathway. Annu Rev Cell Dev Biol 12**:** 393-416.
1387 Blake-Hedges, C., and T. L. Megraw, 2019 Coordination of Embryogenesis by the Centrosome in
1388 Drosophila melanogaster. Results Probl Cell Differ 67**:** 277-321.
1389 Breitwieser, W., F. H. Markussen, H. Horstmann and A. Ephrussi, 1996 Oskar protein interaction
1390 with Vasa represents an essential step in polar granule assembly. Genes Dev 10**:** 2179-
1391 2188.
1392 Brennan, C. A., and K. V. Anderson, 2004 Drosophila: the genetics of innate immune recognition
1393 and response. Annu Rev Immunol 22**:** 457-483.
1394 Brown, J. B., N. Boley, R. Eisman, G. E. May, M. H. Stoiber *et al.*, 2014 Diversity and dynamics
1395 of the Drosophila transcriptome. Nature 512**:** 393-399.
1396 Buchon, N., N. Silverman and S. Cherry, 2014 Immunity in Drosophila melanogaster--from
1397 microbial recognition to whole-organism physiology. Nat Rev Immunol 14**:** 796-810.
1398 Cao, W. X., S. Kabelitz, M. Gupta, E. Yeung, S. Lin *et al.*, 2020 Precise Temporal Regulation of
1399 Post-transcriptional Repressors Is Required for an Orderly Drosophila Maternal-to-Zygotic
1400 Transition. Cell Rep 31**:** 107783.
1401 Cao, W. X., A. Karaiskakis, S. Lin, S. Angers and H. D. Lipshitz, 2022 The F-box protein Bard
1402 (CG14317) targets the Smaug RNA-binding protein for destruction during the Drosophila
1403 maternal-to-zygotic transition. Genetics 220.
1404 Casas-Vila, N., A. Bluhm, S. Sayols, N. Dinges, M. Dejung *et al.*, 2017 The developmental
1405 proteome of Drosophila melanogaster. Genome Res 27**:** 1273-1285.
1406 Cavey, M., and T. Lecuit, 2008 Imaging cellular and molecular dynamics in live embryos using
1407 fluorescent proteins. Methods Mol Biol 420**:** 219-238.
1408 Chang, Y. C., W. T. Hung, Y. C. Chang, H. C. Chang, C. L. Wu *et al.*, 2011 Pathogenic
1409 VCP/TER94 alleles are dominant actives and contribute to neurodegeneration by altering
1410 cellular ATP level in a Drosophila IBMPFD model. PLoS Genet 7**:** e1001288.
1411 Chen, Z. X., D. Sturgill, J. Qu, H. Jiang, S. Park *et al.*, 2014 Comparative validation of the D.
1412 melanogaster modENCODE transcriptome annotation. Genome Res 24**:** 1209-1223.
1413 Chu, K. T., X. H. Niu and L. T. Williams, 1995 A Fas-Associated Protein Factor, Faf1, Potentiates
1414 Fas-Mediated Apoptosis. Proceedings of the National Academy of Sciences of the United
1415 States of America 92**:** 11894-11898.
1416 Colonnetta, M. M., P. Schedl and G. Deshpande, 2023 Germline/soma distinction in Drosophila
1417 embryos requires regulators of zygotic genome activation. Elife 12.

1418 Cunha-Ferreira, I., A. Rodrigues-Martins, I. Bento, M. Riparbelli, W. Zhang *et al.*, 2009 The
1419 SCF/Slimb ubiquitin ligase limits centrosome amplification through degradation of
1420 SAK/PLK4. Curr Biol 19**:** 43-49.
1421 Dahanukar, A., J. A. Walker and R. P. Wharton, 1999 Smaug, a novel RNA-binding protein that
1422 operates a translational switch in Drosophila. Mol Cell 4**:** 209-218.
1423 Dai, R. M., E. Chen, D. L. Longo, C. M. Gorbea and C. C. Li, 1998 Involvement of valosin-
1424 containing protein, an ATPase Co-purified with IkappaBalpha and 26 S proteasome, in
1425 ubiquitin-proteasome-mediated degradation of IkappaBalpha. J Biol Chem 273**:** 3562-
1426 3573.
1427 De Zio, D., E. Ferraro, M. D'Amelio, V. Simoni, M. Bordi *et al.*, 2008 Faf1 is expressed during
1428 neurodevelopment and is involved in Apaf1-dependent caspase-3 activation in proneural
1429 cells. Cell Mol Life Sci 65**:** 1780-1790.
1430 DeHaan, H., A. McCambridge, B. Armstrong, C. Cruse, D. Solanki *et al.*, 2017 An in vivo
1431 proteomic analysis of the Me31B interactome in Drosophila germ granules. FEBS Lett
1432 591**:** 3536-3547.
1433 Deshpande, G., E. Willis, S. Chatterjee, R. Fernandez, K. Dias *et al.*, 2014 BMP signaling and the
1434 maintenance of primordial germ cell identity in Drosophila embryos. PLoS One 9**:** e88847.
1435 Ephrussi, A., and R. Lehmann, 1992 Induction of germ cell formation by oskar. Nature 358**:** 387-
1436 392.
1437 Ewens, C. A., S. Panico, P. Kloppsteck, C. McKeown, I. O. Ebong *et al.*, 2014 The p97-FAF1
1438 protein complex reveals a common mode of p97 adaptor binding. J Biol Chem 289**:** 12077-
1439 12084.
1440 Govind, S., 1999 Control of development and immunity by rel transcription factors in Drosophila.
1441 Oncogene 18**:** 6875-6887.
1442 Griciuc, A., L. Aron, M. J. Roux, R. Klein, A. Giangrande *et al.*, 2010 Inactivation of VCP/ter94
1443 suppresses retinal pathology caused by misfolded rhodopsin in Drosophila. PLoS Genet 6.
1444 Higashiyama, H., F. Hirose, M. Yamaguchi, Y. H. Inoue, N. Fujikake *et al.*, 2002 Identification
1445 of ter94, Drosophila VCP, as a modulator of polyglutamine-induced neurodegeneration.
1446 Cell Death Differ 9**:** 264-273.
1447 Hoffmann, J. A., and J. M. Reichhart, 2002 Drosophila innate immunity: an evolutionary
1448 perspective. Nat Immunol 3**:** 121-126.
1449 Hultmark, D., 1993 Immune reactions in Drosophila and other insects: a model for innate
1450 immunity. Trends Genet 9**:** 178-183.
1451 Huynh, J. R., and D. St Johnston, 2004 The origin of asymmetry: early polarisation of the
1452 Drosophila germline cyst and oocyte. Curr Biol 14**:** R438-449.
1453 Imler, J. L., and J. A. Hoffmann, 2000 Signaling mechanisms in the antimicrobial host defense of
1454 Drosophila. Curr Opin Microbiol 3**:** 16-22.
1455 Jentsch, S., and S. Rumpf, 2007 Cdc48 (p97): a "molecular gearbox" in the ubiquitin pathway?
1456 Trends Biochem Sci 32**:** 6-11.
1457 Jeske, M., B. Moritz, A. Anders and E. Wahle, 2011 Smaug assembles an ATP-dependent stable
1458 complex repressing nanos mRNA translation at multiple levels. EMBO J 30**:** 90-103.
1459 Jones, J. R., and P. M. Macdonald, 2007 Oskar controls morphology of polar granules and nuclear
1460 bodies in Drosophila. Development 134**:** 233-236.
1461 Jongens, T. A., L. D. Ackerman, J. R. Swedlow, L. Y. Jan and Y. N. Jan, 1994 Germ cell-less
1462 encodes a cell type-specific nuclear pore-associated protein and functions early in the
1463 germ-cell specification pathway of Drosophila. Genes Dev 8**:** 2123-2136.

1464 Jongens, T. A., B. Hay, L. Y. Jan and Y. N. Jan, 1992 The germ cell-less gene product: a posteriorly
1465 localized component necessary for germ cell development in Drosophila. Cell 70: 569-584.
1466 Kim, G., C. I. Pai, K. Sato, M. D. Person, A. Nakamura *et al.*, 2015 Region-specific activation of
1467 oskar mRNA translation by inhibition of Bruno-mediated repression. PLoS Genet 11:
1468 e1004992.
1469 Kim, H., H. Zhang, D. Meng, G. Russell, J. N. Lee *et al.*, 2013 UAS domain of Ubxd8 and FAF1
1470 polymerizes upon interaction with long-chain unsaturated fatty acids. J Lipid Res 54: 2144-
1471 2152.
1472 Kim, M., J. H. Lee, S. Y. Lee, E. Kim and J. Chung, 2006 Caspar, a suppressor of antibacterial
1473 immunity in Drosophila. Proceedings of the National Academy of Sciences of the United
1474 States of America 103: 16358-16363.
1475 Kim-Ha, J., J. L. Smith and P. M. Macdonald, 1991 oskar mRNA is localized to the posterior pole
1476 of the Drosophila oocyte. Cell 66: 23-35.
1477 Kloppsteck, P., C. A. Ewens, A. Forster, X. Zhang and P. S. Freemont, 2012 Regulation of p97 in
1478 the ubiquitin-proteasome system by the UBX protein-family. Biochim Biophys Acta 1823:
1479 125-129.
1480 Kubikova, J., G. Ubartaite, J. Metz and M. Jeske, 2023 Structural basis for binding of Drosophila
1481 Smaug to the GPCR Smoothened and to the germline inducer Oskar. Proc Natl Acad Sci
1482 U S A 120: e2304385120.
1483 Kushimura, Y., T. Tokuda, Y. Azuma, I. Yamamoto, I. Mizuta *et al.*, 2018 Overexpression of
1484 ter94, Drosophila VCP, improves motor neuron degeneration induced by knockdown of
1485 TBPH, Drosophila TDP-43. Am J Neurodegener Dis 7: 11-31.
1486 Lattao, R., L. Kovacs and D. M. Glover, 2017 The Centrioles, Centrosomes, Basal Bodies, and
1487 Cilia of Drosophila melanogaster. Genetics 206: 33-53.
1488 Lecuyer, E., H. Yoshida, N. Parthasarathy, C. Alm, T. Babak *et al.*, 2007 Global analysis of mRNA
1489 localization reveals a prominent role in organizing cellular architecture and function. Cell
1490 131: 174-187.
1491 Lee, J. J., J. K. Park, J. Jeong, H. Jeon, J. B. Yoon *et al.*, 2013 Complex of Fas-associated factor 1
1492 (FAF1) with valosin-containing protein (VCP)-Npl4-Ufd1 and polyubiquitinated proteins
1493 promotes endoplasmic reticulum-associated degradation (ERAD). J Biol Chem 288: 6998-
1494 7011.
1495 Lehmann, R., 2016 Germ Plasm Biogenesis--An Oskar-Centric Perspective. Curr Top Dev Biol
1496 116: 679-707.
1497 Lemaitre, B., and J. Hoffmann, 2007 The host defense of Drosophila melanogaster. Annu Rev
1498 Immunol 25: 697-743.
1499 Lerit, D. A., and E. R. Gavis, 2011 Transport of germ plasm on astral microtubules directs germ
1500 cell development in Drosophila. Curr Biol 21: 439-448.
1501 Lerit, D. A., C. W. Shebelut, K. J. Lawlor, N. M. Rusan, E. R. Gavis *et al.*, 2017 Germ Cell-less
1502 Promotes Centrosome Segregation to Induce Germ Cell Formation. Cell Rep 18: 831-839.
1503 Li, J. M., H. Wu, W. Zhang, M. R. Blackburn and J. Jin, 2014 The p97-UFD1L-NPL4 protein
1504 complex mediates cytokine-induced IkappaBalpha proteolysis. Mol Cell Biol 34: 335-347.
1505 Mahowald, A. P., 2001 Assembly of the Drosophila germ plasm. Int Rev Cytol 203: 187-213.
1506 Margottin-Goguet, F., J. Y. Hsu, A. Loktev, H. M. Hsieh, J. D. Reimann *et al.*, 2003 Prophase
1507 destruction of Emi1 by the SCF(betaTrCP/Slimb) ubiquitin ligase activates the anaphase
1508 promoting complex to allow progression beyond prometaphase. Dev Cell 4: 813-826.
1509 Medzhitov, R., 2001 Toll-like receptors and innate immunity. Nat Rev Immunol 1: 135-145.

1510 Menges, C. W., D. A. Altomare and J. R. Testa, 2009 FAS-associated factor 1 (FAF1) Diverse
1511 functions and implications for oncogenesis. Cell Cycle 8**:** 2528-2534.
1512 Meyer, H., M. Bug and S. Bremer, 2012 Emerging functions of the VCP/p97 AAA-ATPase in the
1513 ubiquitin system. Nat Cell Biol 14**:** 117-123.
1514 Meyer, H. H., 2005 Golgi reassembly after mitosis: the AAA family meets the ubiquitin family.
1515 Biochim Biophys Acta 1744**:** 108-119.
1516 Meyer, H. H., J. G. Shorter, J. Seemann, D. Pappin and G. Warren, 2000 A complex of mammalian
1517 ufd1 and npl4 links the AAA-ATPase, p97, to ubiquitin and nuclear transport pathways.
1518 EMBO J 19**:** 2181-2192.
1519 Min-Young, P., M. Ji-Hyun and K. Eunhee, 2004 Fas associated factor 1, FAF1, impairs NF-
1520 kappaB activation by interacting with the IkappaB kinase complex. Molecular Biology of
1521 the Cell 15**:** 2544-2549.
1522 Morais-de-Sa, E., A. Vega-Rioja, V. Trovisco and D. St Johnston, 2013 Oskar is targeted for
1523 degradation by the sequential action of Par-1, GSK-3, and the SCF(-)Slimb ubiquitin
1524 ligase. Dev Cell 26**:** 303-314.
1525 Muers, M., 2011 Functional genomics: the modENCODE guide to the genome. Nat Rev Genet 12**:**
1526 80.
1527 Murphy, T. D., 2003 Drosophila skpA, a component of SCF ubiquitin ligases, regulates
1528 centrosome duplication independently of cyclin E accumulation. J Cell Sci 116**:** 2321-
1529 2332.
1530 Nakamura, A., K. Sato and K. Hanyu-Nakamura, 2004 Drosophila cup is an eIF4E binding protein
1531 that associates with Bruno and regulates oskar mRNA translation in oogenesis. Dev Cell
1532 6**:** 69-78.
1533 Nusslein-Volhard, C., and E. Wieschaus, 1980 Mutations affecting segment number and polarity
1534 in Drosophila. Nature 287**:** 795-801.
1535 Pae, J., R. M. Cinalli, A. Marzio, M. Pagano and R. Lehmann, 2017 GCL and CUL3 Control the
1536 Switch between Cell Lineages by Mediating Localized Degradation of an RTK. Dev Cell
1537 42**:** 130-142 e137.
1538 Park, M. Y., J. H. Moon, K. S. Lee, H. I. Choi, J. Chung *et al.*, 2007 FAF1 suppresses I kappa B
1539 kinase (IKK) activation by disrupting the IKK complex assembly. Journal of Biological
1540 Chemistry 282**:** 27572-27577.
1541 Peters, J. M., M. J. Walsh and W. W. Franke, 1990 An abundant and ubiquitous homo-oligomeric
1542 ring-shaped ATPase particle related to the putative vesicle fusion proteins Sec18p and
1543 NSF. EMBO J 9**:** 1757-1767.
1544 Phuong Thao, D. T., H. Ida, H. Yoshida and M. Yamaguchi, 2006 Identification of the Drosophila
1545 skpA gene as a novel target of the transcription factor DREF. Exp Cell Res 312**:** 3641-
1546 3650.
1547 Raff, J. W., and D. M. Glover, 1989 Centrosomes, and not nuclei, initiate pole cell formation in
1548 Drosophila embryos. Cell 57**:** 611-619.
1549 Reim, G., M. Hruzova, S. Goetze and K. Basler, 2014 Protection of armadillo/beta-Catenin by
1550 armless, a novel positive regulator of wingless signaling. PLoS Biol 12**:** e1001988.
1551 Rogers, G. C., N. M. Rusan, D. M. Roberts, M. Peifer and S. L. Rogers, 2009 The SCF Slimb
1552 ubiquitin ligase regulates Plk4/Sak levels to block centriole reduplication. J Cell Biol 184**:**
1553 225-239.
1554 Roth, S., 2023 Neofunctionalization of Toll Signaling in Insects: From Immunity to Dorsoventral
1555 Patterning. Annu Rev Cell Dev Biol 39**:** 1-22.

1556 Ruden, D. M., V. Sollars, X. Wang, D. Mori, M. Alterman *et al.*, 2000 Membrane fusion proteins
1557 are required for oskar mRNA localization in the Drosophila egg chamber. Dev Biol 218**:**
1558 314-325.
1559 Ryu, S. W., and E. Kim, 2001 Apoptosis induced by human Fas-associated factor 1, hFAF1,
1560 requires its ubiquitin homologous domain, but not the Fas-binding domain. Biochem
1561 Biophys Res Commun 286**:** 1027-1032.
1562 Ryu, S. W., S. J. Lee, M. Y. Park, J. Jun, Y. K. Jung *et al.*, 2003 Fas-associated factor 1, FAF1, is
1563 a member of Fas death-inducing signaling complex. Journal of Biological Chemistry 278**:**
1564 24003-24010.
1565 Schier, A. F., 2007 The maternal-zygotic transition: death and birth of RNAs. Science 316**:** 406-
1566 407.
1567 Schuberth, C., and A. Buchberger, 2008 UBX domain proteins: major regulators of the AAA
1568 ATPase Cdc48/p97. Cell Mol Life Sci 65**:** 2360-2371.
1569 Siddiqui, N. U., A. Karaiskakis, A. L. Goldman, W. V. I. Eagle, C. A. Smibert *et al.*, 2023 Smaug
1570 regulates germ plasm synthesis and primordial germ cell number in Drosophila embryos
1571 by repressing the oskar and bruno 1 mRNAs. bioRxiv.
1572 Snee, M. J., and P. M. Macdonald, 2004 Live imaging of nuage and polar granules: evidence
1573 against a precursor-product relationship and a novel role for Oskar in stabilization of polar
1574 granule components. J Cell Sci 117**:** 2109-2120.
1575 Song, E. J., S. H. Yim, E. Kim, N. S. Kim and K. J. Lee, 2005 Human Fas-associated factor 1,
1576 interacting with ubiquitinated proteins and valosin-containing protein, is involved in the
1577 ubiquitin-proteasome pathway. Mol Cell Biol 25**:** 2511-2524.
1578 Song, J., J. K. Park, J. J. Lee, Y. S. Choi, K. S. Ryu *et al.*, 2009 Structure and interaction of
1579 ubiquitin-associated domain of human Fas-associated factor 1. Protein Sci 18**:** 2265-2276.
1580 Tendulkar, S., S. Hegde, L. Garg, A. Thulasidharan, B. Kaduskar *et al.*, 2022 Caspar, an adapter
1581 for VAPB and TER94, modulates the progression of ALS8 by regulating IMD/NFkappaB-
1582 mediated glial inflammation in a Drosophila model of human disease. Hum Mol Genet 31**:**
1583 2857-2875.
1584 Thibault, S. T., M. A. Singer, W. Y. Miyazaki, B. Milash, N. A. Dompe *et al.*, 2004 A
1585 complementary transposon tool kit for Drosophila melanogaster using P and piggyBac. Nat
1586 Genet 36**:** 283-287.
1587 Thomson, T., N. Liu, A. Arkov, R. Lehmann and P. Lasko, 2008 Isolation of new polar granule
1588 components in Drosophila reveals P body and ER associated proteins. Mech Dev 125**:** 865-
1589 873.
1590 Thulasidharan, A., L. Garg, S. Tendulkar and G. S. Ratnaparkhi, 2024 Age-dependent dynamics
1591 of neuronal VAPB(ALS) inclusions in the adult brain. BioRxiv.
1592 Tomancak, P., A. Beaton, R. Weiszmann, E. Kwan, S. Shu *et al.*, 2002 Systematic determination
1593 of patterns of gene expression during Drosophila embryogenesis. Genome Biol 3**:**
1594 RESEARCH0088.
1595 Valanne, S., J. H. Wang and M. Ramet, 2011 The Drosophila Toll signaling pathway. J Immunol
1596 186**:** 649-656.
1597 Vanzo, N., A. Oprins, D. Xanthakis, A. Ephrussi and C. Rabouille, 2007 Stimulation of
1598 endocytosis and actin dynamics by Oskar polarizes the Drosophila oocyte. Dev Cell 12**:**
1599 543-555.
1600 Wang, L., and P. Ligoxygakis, 2006 Pathogen recognition and signalling in the Drosophila innate
1601 immune response. Immunobiology 211**:** 251-261.

1602 Weiszmann, R., A. S. Hammonds and S. E. Celniker, 2009 Determination of gene expression
1603 patterns using high-throughput RNA in situ hybridization to whole-mount Drosophila
1604 embryos. Nat Protoc 4**:** 605-618.
1605 Wilk, R., J. Hu, D. Blotsky and H. M. Krause, 2016 Diverse and pervasive subcellular distributions
1606 for both coding and long noncoding RNAs. Genes Dev 30**:** 594-609.
1607 Williams, M. J., 2007 Drosophila hemopoiesis and cellular immunity. J Immunol 178**:** 4711-4716.
1608 Wojcik, E. J., D. M. Glover and T. S. Hays, 2000 The SCF ubiquitin ligase protein slimb regulates
1609 centrosome duplication in Drosophila. Curr Biol 10**:** 1131-1134.
1610 Wu, J., and A. Akhmanova, 2017 Microtubule-Organizing Centers. Annu Rev Cell Dev Biol 33**:**
1611 51-75.
1612 Ye, Y., 2006 Diverse functions with a common regulator: ubiquitin takes command of an AAA
1613 ATPase. J Struct Biol 156**:** 29-40.
1614 Zaessinger, S., I. Busseau and M. Simonelig, 2006 Oskar allows nanos mRNA translation in
1615 Drosophila embryos by preventing its deadenylation by Smaug/CCR4. Development 133**:**
1616 4573-4583.
1617 Zeng, Z., D. J. de Gorter, M. Kowalski, P. ten Dijke and O. Shimmi, 2014 Ter94/VCP is a novel
1618 component involved in BMP signaling. PLoS One 9**:** e114475.
1619 Zhang, L., F. Zhou, T. van Laar, J. Zhang, H. van Dam *et al.*, 2011 Fas-associated factor 1
1620 antagonizes Wnt signaling by promoting beta-catenin degradation. Mol Biol Cell 22**:** 1617-
1621 1624.
1622 Zhang, Y., U. Werling and W. Edelmann, 2012 SLiCE: a novel bacterial cell extract-based DNA
1623 cloning method. Nucleic Acids Res 40**:** e55.
1624 Zhang, Y., U. Werling and W. Edelmann, 2014 Seamless Ligation Cloning Extract (SLiCE)
1625 cloning method. Methods Mol Biol 1116**:** 235-244.
1626

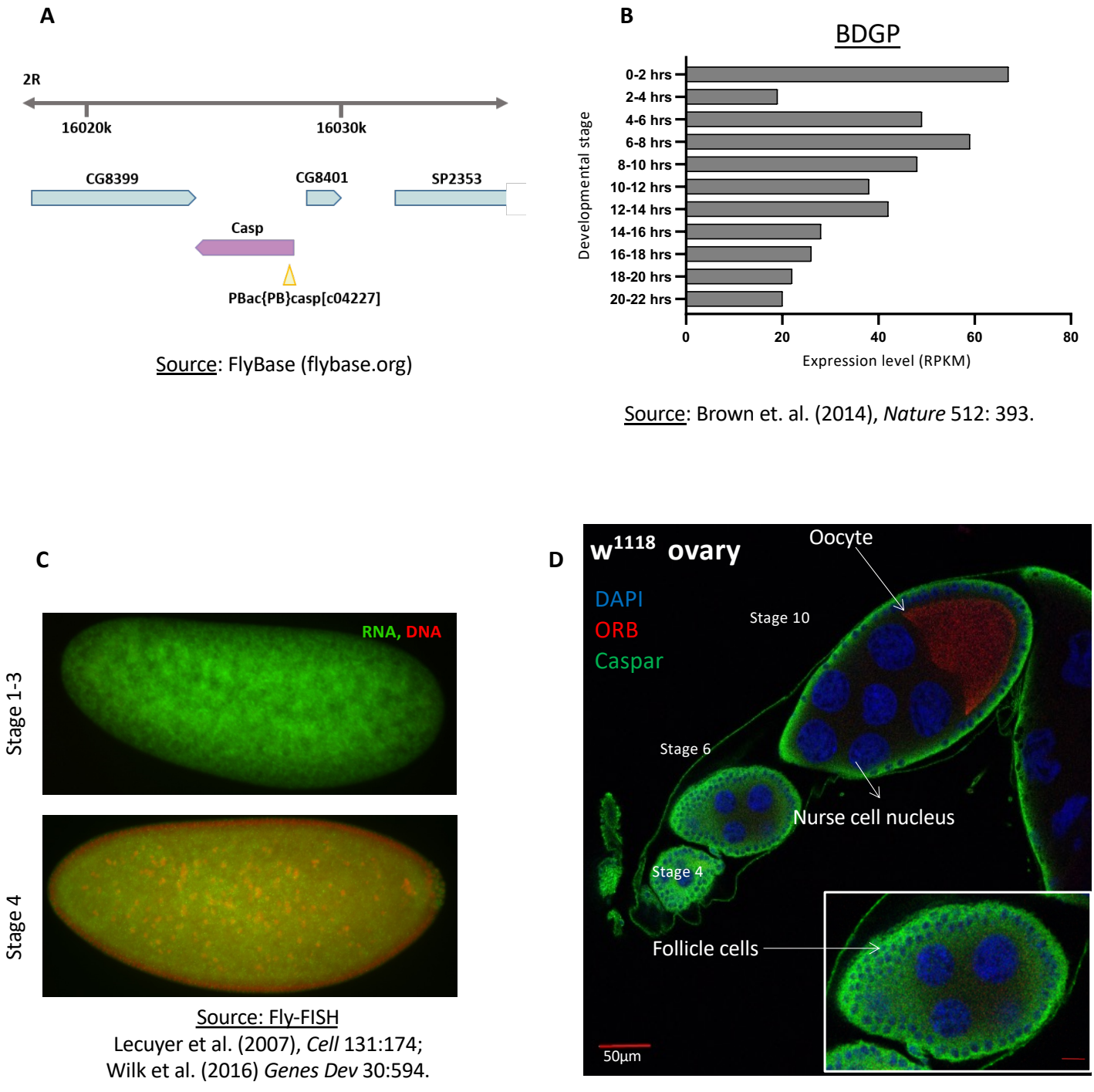

Fig. S1. **(A)** Schematic of the the chromosomal location of the *casp* locus and the associated transposon insertion that generates the *casp*^{c04227} allele. This allele is referred to as *casp*^{lof} hereafter. **(B)** RNA expression data from the modENCODE database, plotted as a bar chart. **(C)** shows RNA-in situ hybridization of *Casp* in the embryo (Fly-FISH). Casp protein staining in the oocyte is depicted in **(D)**. DAPI marks the nuclei, orb marks the oocyte. Casp marks the follicle cells, but is not significantly enriched in the germline (egg, nurse cells).

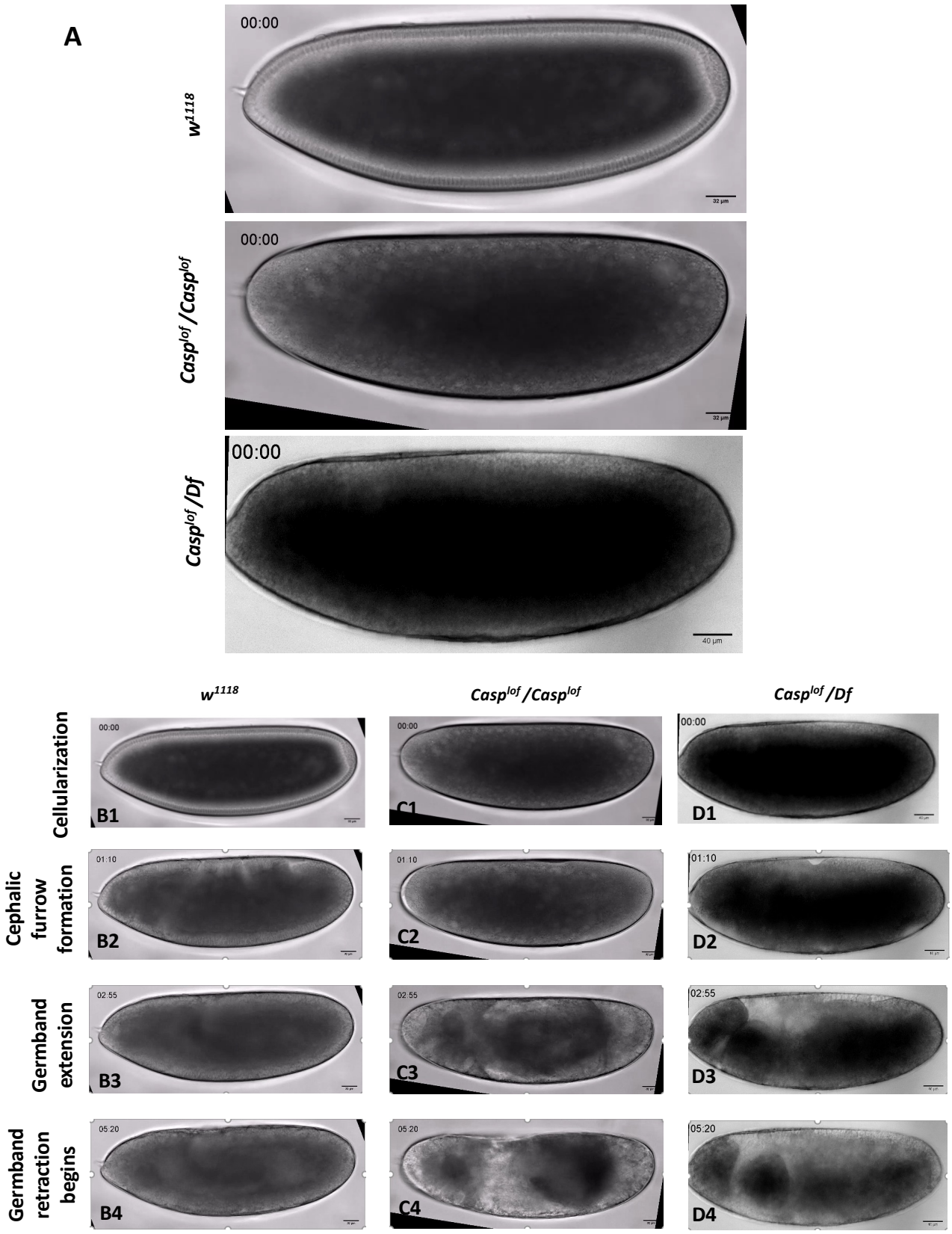

Fig. S2. *Casp* assists in progression to gastrulation.
(A) Representative movies for the early development of the indicated genotypes are shown in D.
(B-D) Time-lapse images are presented for the wild-type and mutants in B1-D4. Out of 96 time points imaged, four are shown for each genotype. Images were acquired from a single, constant plane unique to each embryo across 5-minute intervals. The developmental trajectory for w^{1118} can be followed from the cellularization stage to the beginning of germ band retraction, for the time points indicated. Crucial developmental milestones are highlighted (B1-B4). *casp* mutants did not exhibit characteristic stages of morphogenesis at comparable time points (C1-C4, D1-D4), n = 10.

A

Protein	Peptide count
casp	73.5
TER94	18
Vap33	2.5
Tudor-SN	2.25
alphaTub85E	2
eIF4A	2
Npl4	2
SERCA	1.75
bel	1.75
CCT2	1.5
mRpS14	1.5
CCT6	1.5
Hacl	1.25
mAcon1	1.25
ATPsyngamma	1.25
mRpL27	1.25
alphaTub67C	1.25
eIF3b	1
ScsbetaA	1
26-29-p	1
lig	1
me31B	1
nocte	1
Ufd1-like	1

C

Protein	Known function in the germline	Reference
TER94	polar granule component; associated with vasa and Tudor	Thomson et al., 2008
Tudor-SN	regulates spermatogenesis	Ku et al., 2016
eIF4A	polar granule component; associated with vasa and Tudor	Thomson et al., 2008
belle	required for female fertility and maintenance of male germline stem cells	Johnstone et al., 2005
CCT6	expressed in primordial germ cells	Fisher et al., 2012
α-Tubulin at 67C	regulation of male germline stem cells, centrosome positioning and segregation	Tao et al., 2021
Lingerer	interacts with germline component vasa	Durdevic and Ephrussi, 2019
me31B	polar granule component; associated with vasa and Tudor	Thomson et al., 2008

B

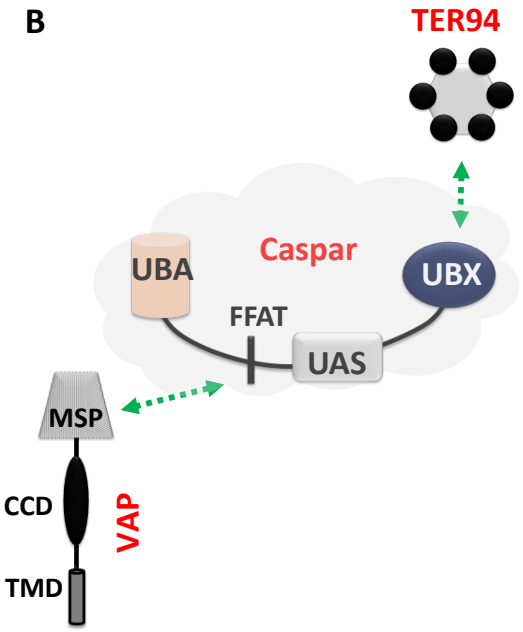

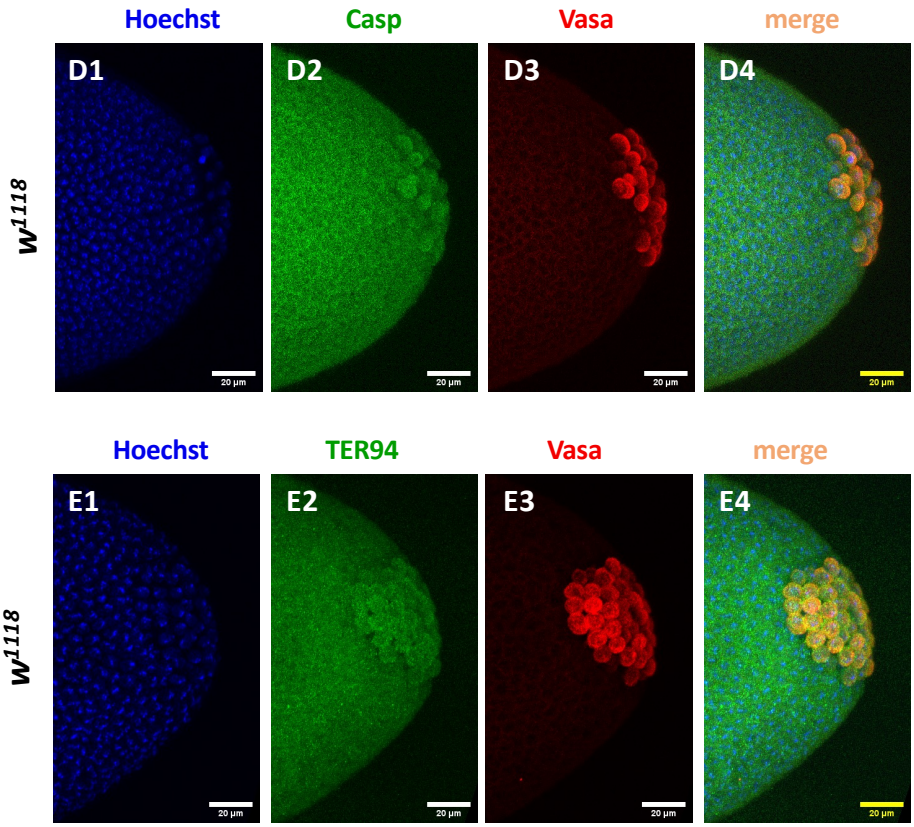

Fig. S3. TER94 and germline components are major interactors of Casp. (**A**) shows a list of the 24 proteins enriched after a Casp IP, followed by mass spectrometry, listed in the order of their peptide counts. The peptide counts are averaged from 4 biological replicates. A subset of interactors with known functions or expression in the germline are tabulated in (**B**) A schematic of the interaction of Casp with both TER94 and VAPB (Tendulkar et al., 2022). TER94 interacts with the Casp UBX domain, while VAPB with the FFAT motif (**C**) List of proteins that are associated with Casp and are previously identified as pole-cell components (**D-E**) Immunostaining of wild-type nuclear cycle 13/14 embryos with Casp (D2) and TER94-specific (E2) antibodies indicates expression in the primordial germ cells (C1-D4). Hoechst marks nuclei and Vasa marks the germ cells.

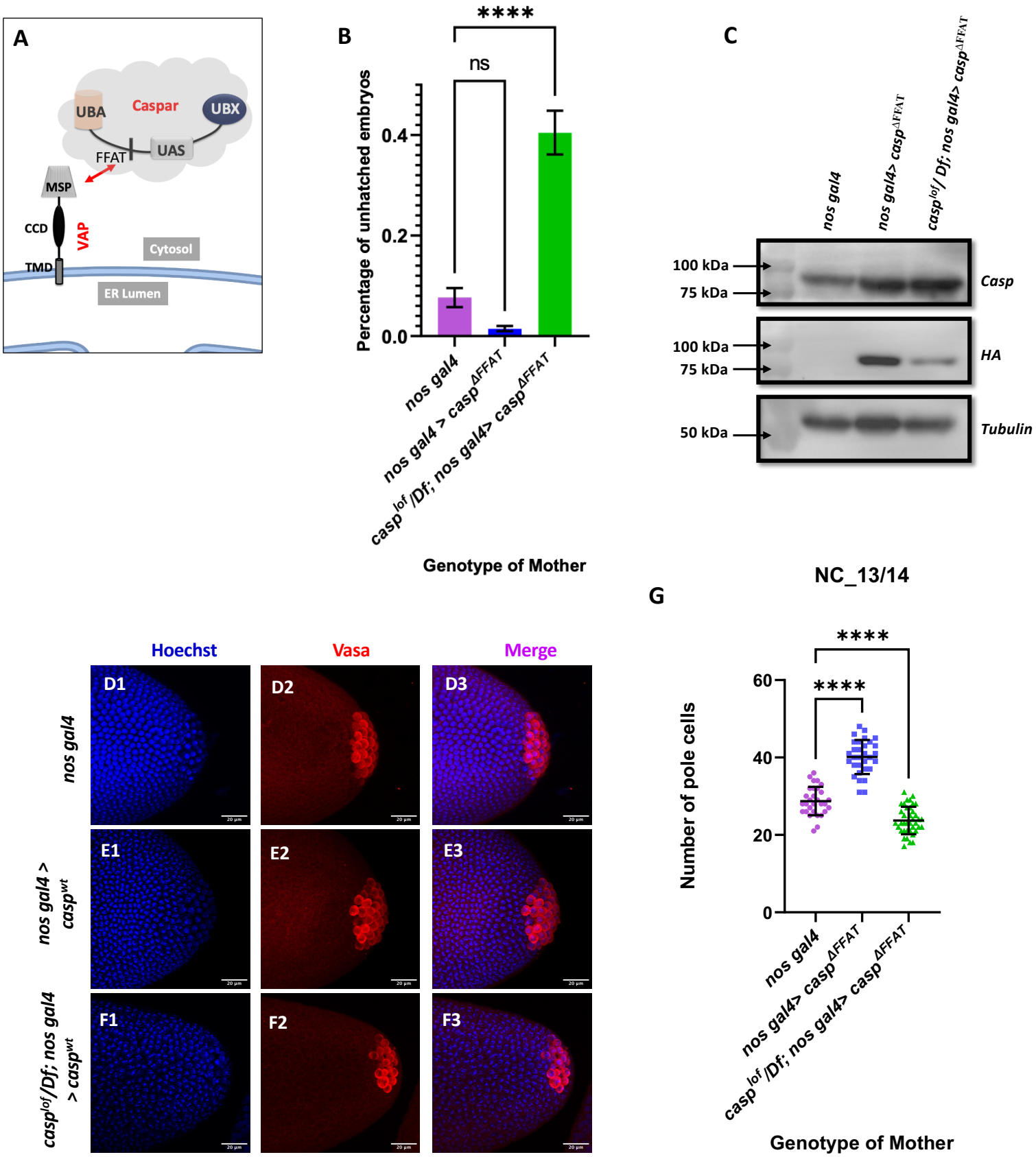

Fig S4. Casp:VAP interaction is not required for defining pole cell number. (**A**) Casp interacts with VAPB via its FFAT-like motif (**B**) represents embryonic lethality at 25° C plotted as a bar graph. The genotype of the mother is listed on the X-axis. N = 3. n = 200, ordinary one-way ANOVA, (****) P <0.0001. (**C**) Casp protein levels were assessed in 0-3h embryos via western blotting. Rabbit anti Casp (1:10,000) and rabbit anti HA (1:2000) antibodies were used to probe the blot. Mouse anti Tubulin (1:10,000)is used as a loading control. (**D-F**) Confocal microscopy images of the posterior of nuclear cycle 13/14 embryos from mated *nos gal4* (D1-D3), *nos gal4> casp$^{\Delta FFAT}$* (E1-E3), and *casp^{lof}/Df; nos gal4> casp$^{\Delta FFAT}$* (F1-F3) females immunostained with vasa antibody (1:50). Hoechst marks the nuclei. (**G**) The germ cells at the posterior marked by vasa quantified and plotted as bar graphs. n = 30-40. Ordinary one-way ANOVA, (****) P <0.0001